EXPERIMENTAL PROCEDURES AND DATA COMPILATION TECHNIQUES FOR ULTRASONIC DOSIMETRIC ANALYSIS

BY

STEVEN CLIFFORD GRADY

B.S., University of Illinois, 1979

THESIS

Submitted in partial fulfillment of the requirements
for the degree of Masters of Science in Electrical Engineering
in the Graduate College of the
University of Illinois at Urbana-Champaign, 1980

Urbana, Illinois

Acknowledgement

The author wishes to express his appreciation to his advisor Dr. W. D. O'Brien for his suggestion of this thesis topic, counsel, and support. Thanks are also extended to Anne Delk and Jeanette Wyneken who assisted tremendously in data acquisition, Charlie Edwards and Kay Bailey for photographic contributions, Wanda Elliot for her technical expertise and typing of parts of this thesis, and Dr. L. Frizzell and Dr. R. Johnston for their advice. Special thanks go to my parents for their support throughout my education and my wife Jodie for her suggestions and patience during the final days.

TABLE OF CONTENTS

Chapter 1

INTRODUCTION

In recent years the use of ultrasound in medical applications has increased dramatically. Projected sales of ultrasonic medical instrumentation should surpass one hundred million dollars by 1985 (Electronics,1979). In an effort to bring new technology to the marketplace, the area of ultrasonic dosimetry has been neglected. Dosimetry is concerned with defining a quantitative relationship between some physical agent and the biological effect it produces. In the case of ultrasound a specific parameter such as intensity, particle displacement, or acoustic pressure for example, would be related to the likelihood of the occurence of a biological alteration, usually located at the same irradiation site. This relationship is not meant to suggest that the clinical use of ultrasound is a hazard. There have been a number of studies though, which show that sufficient levels of ultrasound can produce irreversible biological damage. The increased clinical employment of ultrasonic instrumentation therefore, demands that information concerning the interaction of ultrasound energy with tissues be obtained.

To accomplish the objective of ultrasonic dosimetry, it is necessary to quantify accurately and precisely the ultrasonic source output parameters, determine in what manner the material effects the propagating energy ,and relate these two items to a quantitative parameter determination at the site of interest. Therefore, the physical quantities which describe an interaction at some biological site must be defined and integrated into a concept that is applicable in ultrasonic radiation protection. The main objective of this thesis is to develop an ultrasonic dosimetric model from which the ultrasonic energy being absorbed or interacting with biological tissue can be determined.

To facilitate this model, the basic procedure will be to detect the distribution of the ultrasonic energy inside the specimen during irradiation. This will be done by first characterizing the complex ultrasonic field distribution patterns in the free field, and then inserting the specimen in the field to measure the *in vivo* field distribution within the specimen using the transient thermoelectric technique (Fry and Fry, 1954a and 1954b). Using this thermocouple technique to measure the tissue absorption coefficient, with a known spatial and temporal intensity and the exposure time, the amount of energy absorbed by the tissue may be found. This absorbed energy distribution with possible units of J/mm**3, can be related directly to the corresponding biological effects. The parameter most widely used in bioeffect and biophysical studies is intensity. Given in mixed units of W/cm**2, intensity is primarily used because it is an easily measured parameter. It is not acceptable as a dosimetric quantity however, because it is an exposure condition, and not a measure of dose.

Some *in vivo* work has been done by other researchers. Most notably, the *in utero* work of (Hall and Robinson,1974) and the *in vivo* work of Bang (1972). A universal dosimetric response to ultrasonic exposure for different tissues has been suggested (Johnston and Dunn, 1976), but was demonstrated in the case of suprathreshold lesions in brain tissue only. The experiment described in this thesis was not concerned with suprathreshold intensities as no biological damage assessment was undertaken. Rather, the philosophy of this work is to examine the interactions between the ultrasonic energy and the tissues, determine tissue characteristics such as the absorption coefficient, and determine the energy absorbed within the specimen. Using the instrumentation and procedures described in the following chapters, a dosimetric model will be developed to find the absorption coefficient and absorbed energy of an irradiated tissue site. Improvements in both the experimental procedure and dosimetric model are proposed in Chapter 5.

CHAPTER 2

INSTRUMENTATION

This chapter details the instrumentation used in this experiment. Associated theory is presented where necessary. The instrumentation may be classified into three main categories 1) the ultrasonic source and associated driving hardware, 2) the thermocouple probe and recording device, and 3) the irradiation apparatus.

Section 2.1 The Ultrasonic Transducer

In the development of this experiment a number of constraints were placed on the acoustic field. First, the transducer must produce a field which can be directed at a particular location in the specimen. Also, for ease of analysis, it would be convenient to assume plane wave geometry at the irradiation site. To satisfy these criteria, a transducer which produces a focused field must be used. It was decided to use an existing focusing lens trasnsducer. Other types of focusing transducers are discussed elsewhere (Fry and Dunn, 1962).

Lens transducers are often constructed in a sandwich arrangement consisting of a piezoelectric crystal, a spacing material, and a plano concave lens. An arrangement of this type is shown in figure 1. In this transducer quartz is used for the oscillating plate. Quartz is often used for the crystal because of its high stability and high tensile strengths compared to ceramic crystals. Quartz has the disadvantage of requiring a relatively high electric field strength to obtain high power outputs due to the high input impedance of quartz. Thus, the power output of a quartz radiator is determined by the crystal and crystal holder.

The spacing material is used as a coupling medium between the crystal and the lens. Its thickness is usually one quarter of a wavelength to assure total transmission. A material this thin also has low sound attenuation. The spacer fluid in this case was Silicon 710 (Dow Corning Midland,Mich.), which was also used behind the transducer to aid in heat conduction.

The lens is a critcal component of the system as it must meet a number of criteria. The lens focuses the sound by the refraction of the wave as it passes through a media of differing sound velocity. However, when there is a refractive index n,

$$n = c_1/c_2 \qquad (1)$$

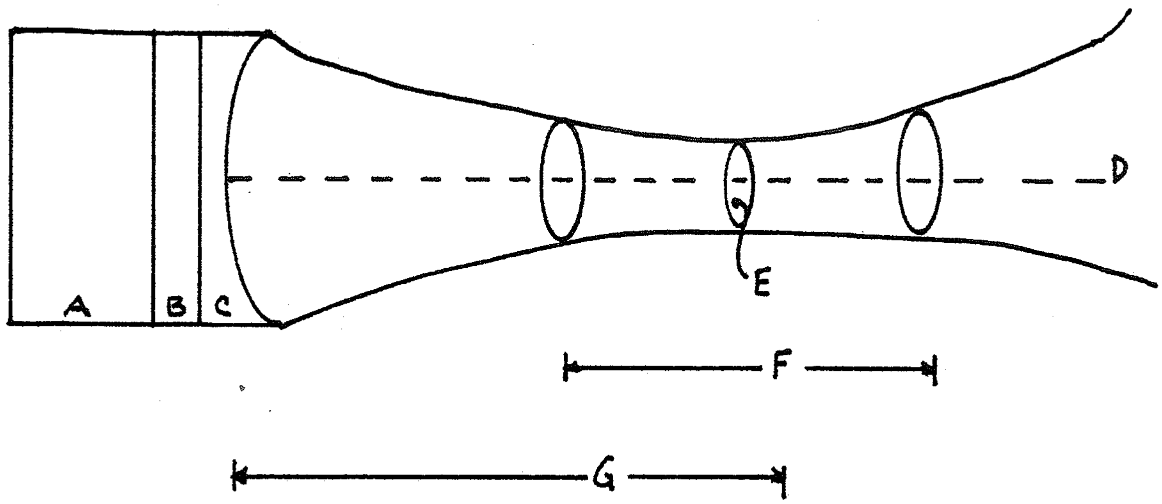

A) QUARTZ OSCILLATOR
B) SPACER MATERIAL
C) LUCITE LENS
D) FOCAL AXIS
E) FOCAL AREA (DIAMETER = Dt)
F) DEPTH OF FOCUS (Da)
G) FOCAL LENGTH (F)

Figure 1. Schematic of transducer with focused field parameters (NEMA/AIUM Safety Standard, 1979)

where c1 and c2 are the sound velocities in medium 1 and medium 2 respectively, there is an impedance discontinuity. This discontinuity may be designated by the ratio of the impedances given by;

$$m = \rho_1 C_1 / \rho_2 C_2 \qquad (2)$$

where $\rho_1 C_1$ is the characteristic impedance of the lens and $\rho_2 C_2$ is the characteristic impedence of the propagating medium. This leads to a reflection coefficient R;

$$R = \left(\frac{\rho_2 C_2 - \rho_1 C_1}{\rho_2 C_2 + \rho_1 C_1} \right)^2 \qquad (3)$$

The conditions for a good lens then must be n 1 and m=1 The material must also be machinable and have a low attenuation coefficient. The lens used in this transducer is Lucite. The characteristic parameters of this lens are ρ =1.18E03 kg/m3, c=2.8E03 m/s, n=1.9, m=2.2 and R=0.14 (Hueter and Bolt,1955). This lens is mounted flush to the spacer/crystal face. This unit is contained in a stainless steel housing with a rear connector to accomodate a shielded high voltage cable.

The driving network used to supply the high voltage necessary to produce oscillation of the transducer crystal is shown in figure 2. This R.F system provides an output on any

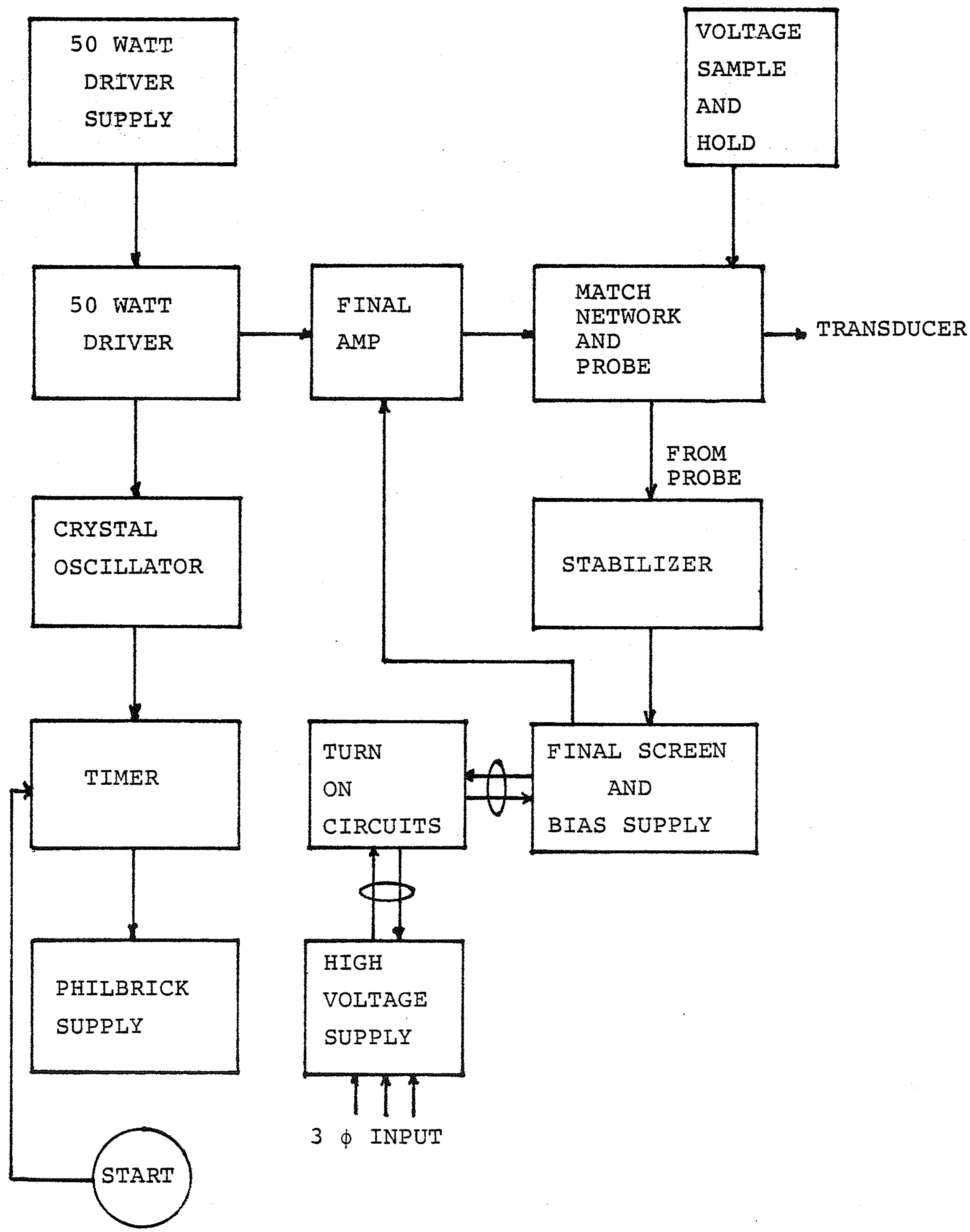

Figure 2. 2 kW driving system block diagram

of several frequencies at an R.F. power level up to 2 kW. It provides a closely controlled envelope (power level) from about 0.5 watts to over 2,000 watts by means of detected negative feedback. Frequencies are selected by means of a switch on the crystal oscillator and by changing several plug in coils. The R.F. frequency used in this experiment was 0.98 MHz which is the resonant frequency of the transducer. All interconnections for R.F. signals are made with matched 50 ohm coaxial cables.

Referring to figure 2, a start command (ground signal) is received by the timer chassis. This chassis generates a square wave pulse with a time duration selected by a front panel switch. The pulse from the time chassis turns on a buffer amplifier in the crystal oscillator chassis. The oscillator is followed by a coarse and fine step attenuator which varies the output of the oscillator chassis from nearly 0 watts to 2 watts. The oscillator chassis drives a 50 watt amplifier, which in turn drives the 2 kW final amplifier. The output from the 2 kW final amplifier is connected to a matching network which transforms the 50 ohm output impedance of the final amplifier to the large input impedance of the transducer. The rectified R.F. (now a changing d.c. level) is connected to a high gain amplifier, the stabilizer. The output of the stabilizer is connected to the 2 kW amplifier screen supply voltage. This causes an increase or decrease in the R.F. envelope in the opposite sense of the original disturbance. This feedback is meant to hold the output of the system to within 0.1% of the desired level. The stabilizer can be connected to the screen supply of the 50 watt driver when the system is used in low level operation.

Included in the matching network is a capacitive voltage divider to produce the transducer driving voltage. The voltage divider ratio may be varied by a precision variable capacitor in the voltage divider. This network provides a means of obtaining variable acoustic intensities by changing the voltage applied to the transducer crystal. This applied voltage is given by the relation;

$$V = 2.86 \times 10^2 + 4.98 * C_s \quad (4)$$

where Cs is the variable capacitor dial setting. The resultant ultrasonic intensity produced by the transducer is described by;

$$I = \left(\frac{V}{V_{CAL}}\right)^2 * I_{CAL} \quad (5)$$

where Ical and Vcal are the calibrated intensity and voltage respectively. These two quantities are determined for the transducer in a process which involves the transient thermoelectric technique and the elastic sphere radiometer (Dunn et al, 1977). In a typical intensity calculation, the voltage obtained with a capacitor setting of Cs=360 is V=2078.8 volts. The resulting intensity produced by this voltage using Ical=5.5 W/cm**2 and Vcal=685 V is I=50.8 W/cm**2. The intensities produced by the transducer in this experiment fall in the range of 10-60 W/cm**2.

It will be assumed for ease of analysis that the quartz plate may be modeled as a plane piston source. The field produced by such a source is mathematically described in a number of texts (Kinsler and Frey, 1962). This field possesses two distinct regions. In this analysis it is assumed that the transducer radius is much greater that than the wavelength. In the near field, known as the Fresnel zone, the axial intensity runs through a series of maxima of constant amplitude with intervening nulls. The last null occurs in the vicinity of d=a**2/2*λ, where d is the axial distance away from the source face, a is the radius of the piston, and λ is the wavelength. At d=a**2/λ the intensity goes through its final maximum and as d>a**2/λ, the intensity decreases inversely as the square of the distance. This region where d>a**2/λ is called the far field or Fraunhofer zone. This complex field pattern has been modeled by a number of authors(Fry and Dunn,1962).

When a plano concave lens is placed over this quartz source, the field structure is changed drastically. The unfocused radiated sound for distances less than a**2/λ may be thought of as being confined within a cylinder of radius a, whereas beyond this point there is at least approximate spherical divergence. On the other hand, the focused field intensity will converge at a designed focal length and then diverge. It is imperative for focusing that the focal length of the lens occurs inside the axial position of the zero order maxima of the unfocused field. This limits the choice of focal length for a particular crystal. In the case of the crystal used in the experimental transducer, the zero order maxima occurs at a**2/λ which is 20 cm. As will be revealed shortly,the actual focal length for this transducer is well below this limit.

Having determined the intensity of the acoustic field, it is of great importance to determine its shape. This shape is determined by a number of lens characteristics. First, the focal length F is given by;

$$F = \frac{r}{1 - 1/n} \qquad (6)$$

where r is the lens radius of curvature, and n is the index of refraction for the lens. This formula is derived from the analogous formulas for optics. It must be noted that the sound velocity in the lens is greater than that of water, so the shape for an ultrasonic converging lens is opposite that for an optical converging lens. Furthermore, the diameter to wavelength ratio is much smaller here than in optical lenses, thus the convergence in the acoustic case will be several orders of magnitude larger. Noting this, and assuming the lens is so thin that the axial length is negligible, equation 6 can be used to find the focal length.

To characterize the "working" part of the focused field, two other parameters are introduced. The schematic representation of these beam profile parameters are shown in figure 2. Dt is defined as the diameter of the focal area. This is the distance between the off axial points that are one half the intensity of the axial point. The relation to find this distance numerically is given by;

$$D_t = k_t \left(F/D \right) * \lambda \qquad (7)$$

where the quantity kt is dimensionless and somewhat dependent upon the half aperture angle ψ. This width Dt is taken in the neighborhood of the focal length and is not applicable further axially from the transducer. The other parameter is the axial length of the depth of focus, Da. This length is the distance between the two axial points which are at one half the maximal axial intensity. Da is given by;

$$D_a = K_a * D_t \qquad (8)$$

where ka is dependent on the half aperture angle. These two approximations may be derived from the fundamental equations presented by O'Neil(1949) after making a few assumptions. First, the point under analysis is a large distance away from the transducer. Secondly, the radius of the transducer is larger than a wavelength. Finally, the intensity distribution is gaussian,so specific values may be found on it. In the case of this particular transducer, it will be shown that all these conditions are satisfied.

It is of great importance to quantify Da and Dt as given above. The lens was measured with a micrometer. From the geometry in figure 3, the radius of curvature was found to be 34.2 mm. From equation 6 the focal length was calculated to be 72.2mm. The half aperture angle ψ measured at the focal point is 13.6 degrees. To find Da and Dt, the k constants must be evaluated. For half aperture angle less than 50 degrees, Dt will be within 20% if kt=1. Therefore, a value for the transverse focal diameter is found to be 3.3 mm. The value of ka is also dependent on the half aperture angle and in this case is about 13 (Fry and Dunn,1962,figure 26). Using this value, the depth of focus should be about 40 mm. In the following chapter these field parameters are determined experimentally, and the resultant values will be compared against those obtained above.

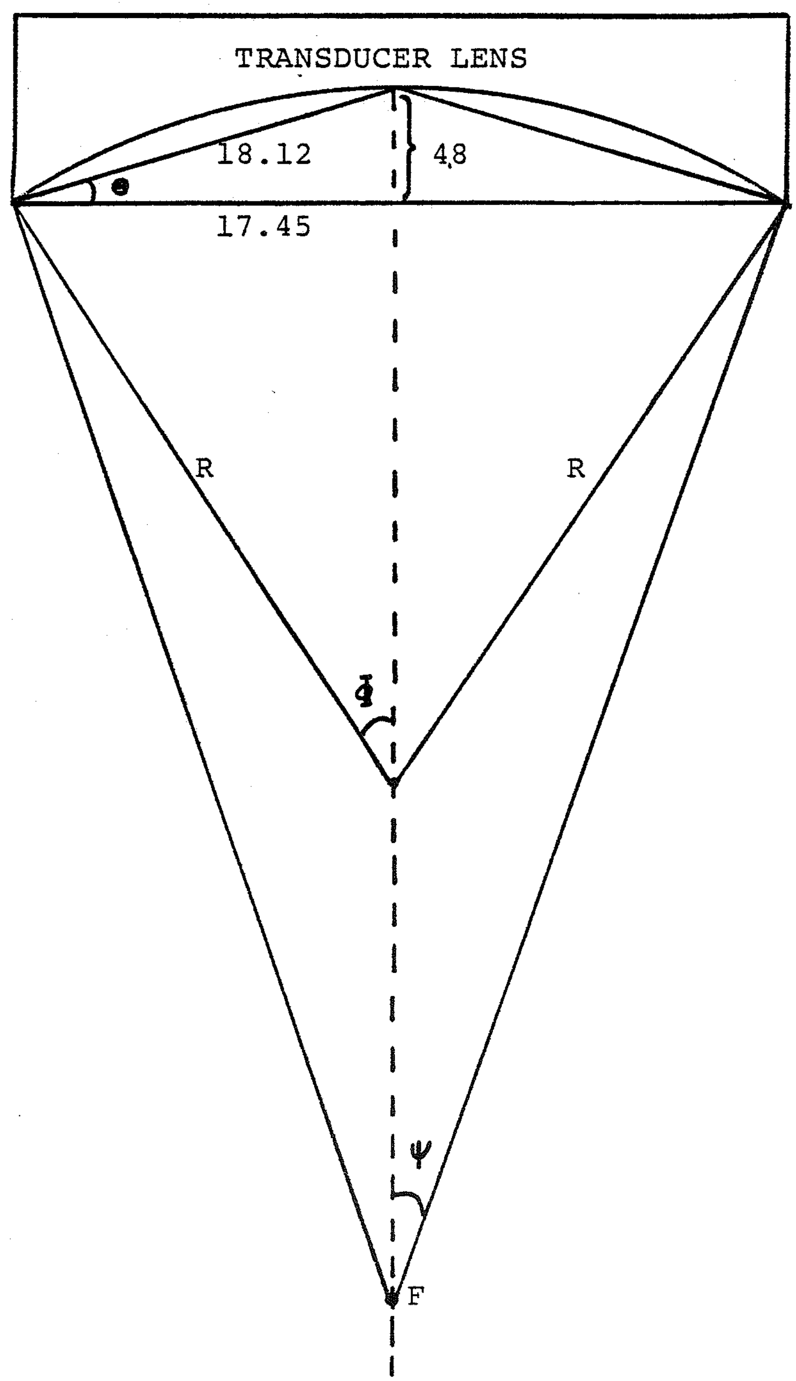

Figure 3. Lens geometry used for calculation of radius of curvature and focal length all lengths are in millimeters

Section 2.2 The Thermocouple Probe

The primary object of this study is to determine the absorption coefficient of an irradiated biological specimen and determine the absorbed energy. The ultrasonic probe which would be used to accomplish this must have a number of qualities. The probe should be small to mimimize the insertion damage to the tissue and not interrupt the ultrasonic beam propagation. Also, the probe should provide a means to obtain a value for absorption only. Furthermore, the probe should be mobile within the specimen to enable analysis at a number of different tissue sites. The only probe available which satisfies these criteria is the thermocouple (Fry and Fry, 1954a and 1954b). The probe consists of two wires of different metals welded or soldered together at one end to form a thermocouple junction. The method involves placing the thermocouple junction in the tissue of interest, and irradiating it with a ultrasonic pulse of known intensity, duration and carrier frequency. This pulse will interact with the tissue in such a manner as to increase the tissue temperature. When this occurs, the emf of the thermocouple will change and a voltage difference will be measured across the thermocouple leads. This difference can be correlated to a time rate of change of tissue temperature. When the acoustic intensity at the junction is known, the following relation can be used to find the absorption coefficient α,

$$\alpha = \frac{\rho C}{2I}\left(\frac{dT}{dt}\right) \qquad (9)$$

where ρ C is the product of the tissue density and heat capacity (J/°Ccm**3), I is the sound intensity (W/cm**2), and (dT/dt) is the initial time rate of temperature(°C/sec). Therefore, from directly measuring (dT/dt), we can obtain a value for the absorption coefficient for the tissue under test.

The typical response of a thermocouple probe to a single acoustic pulse having a one second rectangular envelope is shown in figure 4. A relatively rapid rise occurs just after the initiation of the pulse followed by a slower "linear" rising phase for the remainder of the one second interval. After cessation of the pulse, a rapid fall in temperature occurs followed by a slower return of the temperature to its value preceeding the acoustic pulse. The initial rapid increase in temperature results from the conversion of acoustic energy into heat by the viscous forces acting between the thermocouple wire and the imbedding medium. This phase of the response approaches equilibrium rapidly. Since the magnitude of this viscous heating depends on the angle of incidence of the sound field with respect to the thermocouple

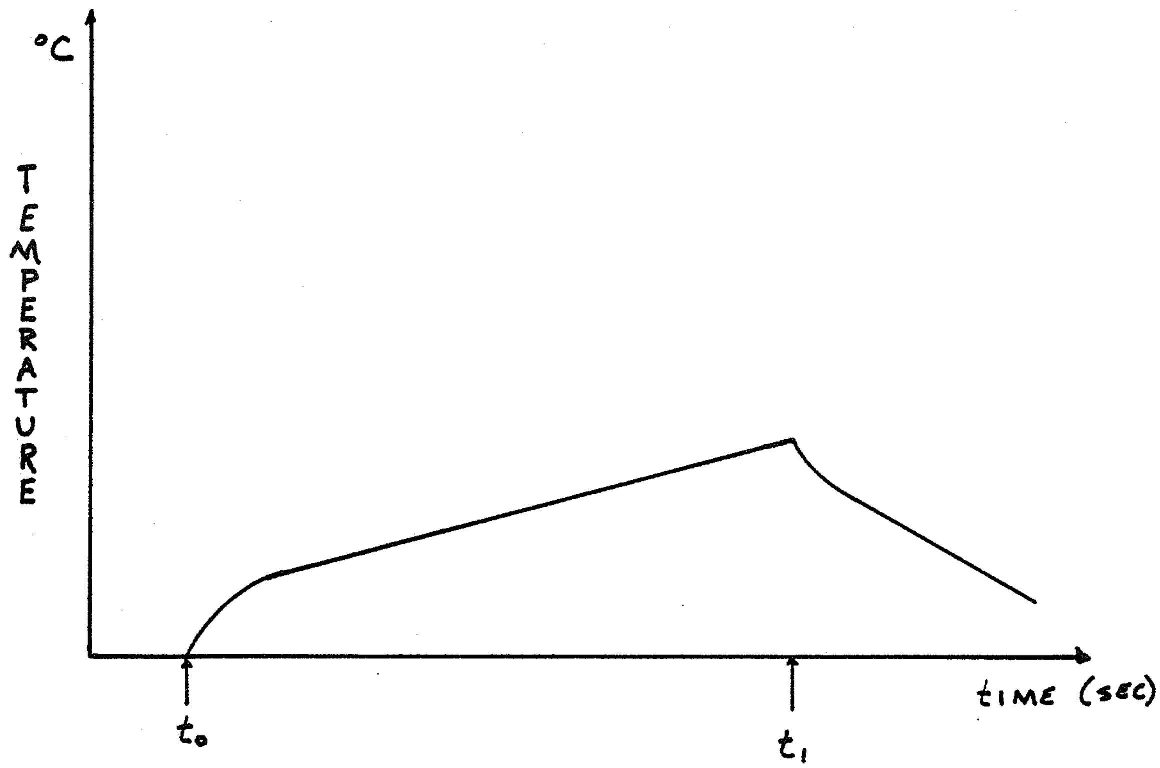

Figure 4. Typical thermocouple response (t_o is time at beginning of acoustic pulse. t_1 is time at end of acoustic pulse.

wire, it is assumed the wire is transverse to the direction of propagation. The second phase of the temperature sequence the "linear" part,is produced by absorption of sound in the body of the imbedding medium. The closeness of approach of this phase to linearity during irradiation is dependent on; 1) the acoustic amplitude; 2) the form of the variation of acoustic absorption coefficient with temperature; 3) the heat conductivity coefficients of the tissue and the wires; 4) the duration of the acoustic disturbance; 5) the acoustic field distribution.

The thermocouple wire size and ultrasonic beam width play a major role in the accuracy of the determination of the absorption coefficient. Different combinations of thermocouple wire diameter and beam widths can produce widely varying thermocouple emf responses, which in turn yield erroneous absorption coefficient values (Goss et al, 1977). It was shown that the use of small diameter wires (13 μm) would minimize errors in the absorption coefficient determination. The use of small diameter wires corresponds to a mechanically weaker junction. As will be seen in Chapter 3, the thermocouple will be subjected to mechanical stress. The junction must be able to withstand this stress for the duration of the experiment. Previous work done in this lab suggested the use of 76 μm diameter wires as a compromise between small diameter and mechanical junction strength. The next section deals with the manufacturing process of a 76 µm diameter thermocouple.

Section 2.2.1 Thermocouple fabrication

As discussed previously, the thermocouple junctions to be used in this experiment must have a number of qualities. A butt welded 76 µm diameter chromel-constantan thermocouple was designed to satisfy these criteria. The design allows for smooth passage through the specimen, has a sensitivity of 60 µV/ C (Omega Temperature Measurement Catalog,1980), can be subjected to experimental stresses without breaking, and uninterruption of the acoustic field may be assumed since the wire radius is much smaller than the wavelength. A magnified view of a 76 µm diameter thermocouple is shown in figure 5. Notice in this photo, the butt weld is well aligned. This junction has no protruding edge which might snag on tissue. The manufacture technique to assure this consistent alignment is as follows.

A square section of 76 µm mylar plastic was sandwiched between a glass slide and coverslip (figure 6). A fingertip held junction manipulator was also fashioned from 76 µm mylar. When the manipulator was inserted under the cover slip, a channel of variable width and 76 µm height was formed. The chromel (Hoskins Mfg Co, Detriot ,Mich.) and

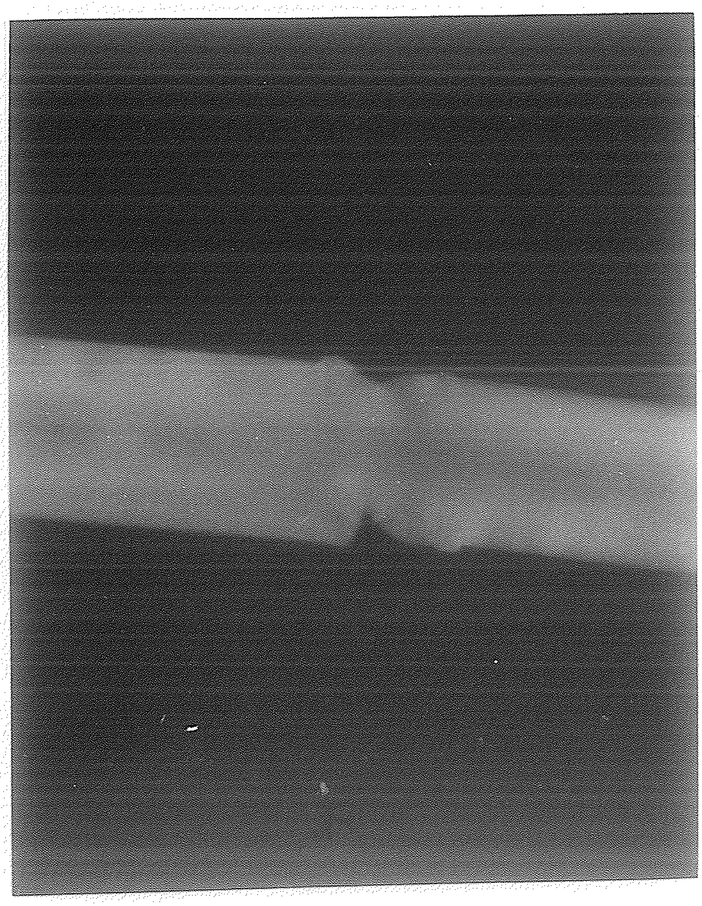

Figure 5. 76 μm thermocouple junction magnified 25x.

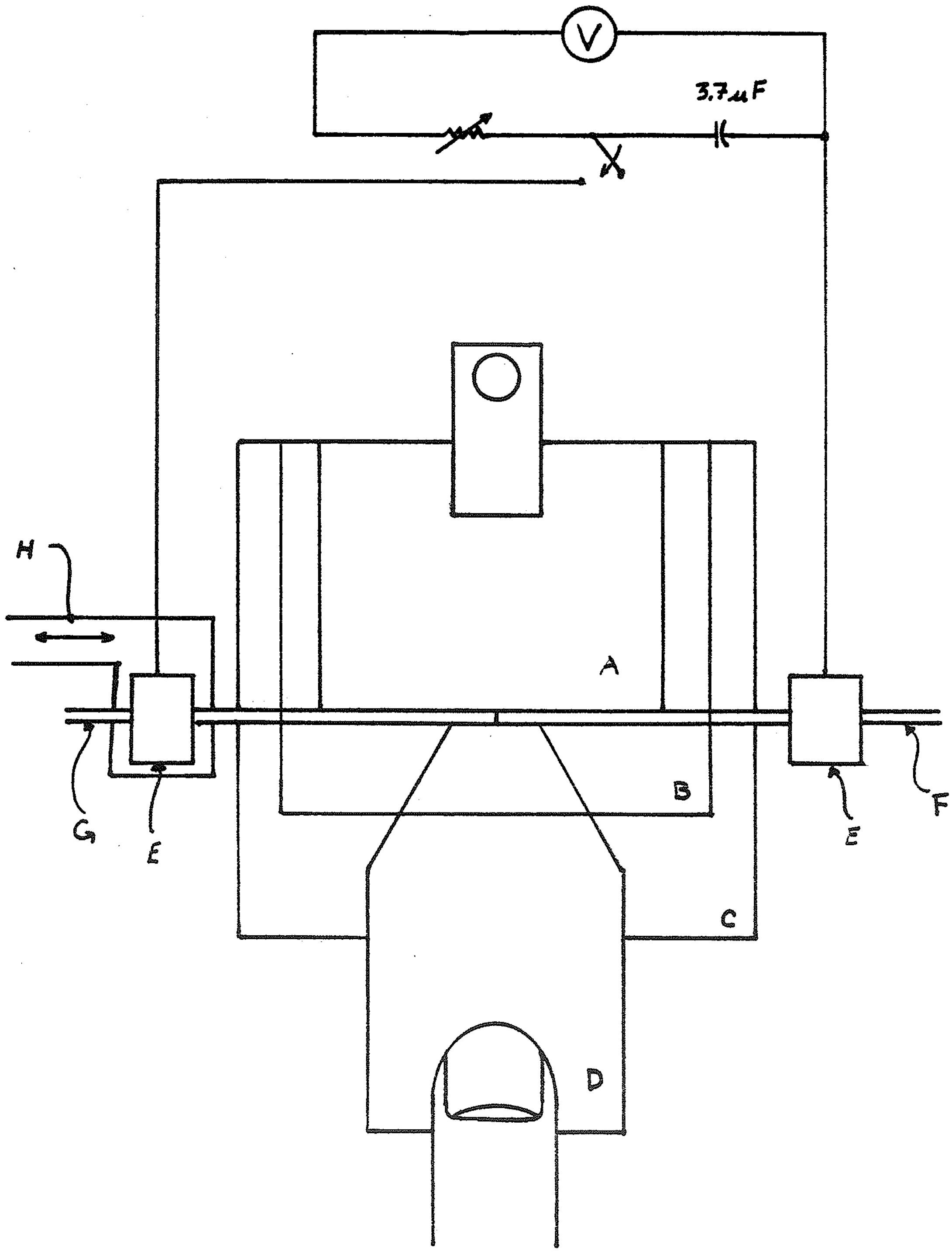

Figure 6. Schematic diagram of thermocouple manufacturing apparatus A) 76 μm mylar sheet, B) coverslip, C) glass slide, D) manipulator, E) clamping block, F) constantan wire, G) chromel wire, H) arm from worm gear

constantan (Cohen Wire Co., Mount Vernon, N.Y.) wires were cut into 15 cm lengths. The constantan wire was inserted under the coverslip from the left. When the tip to be welded was approximately at the midpoint of the channel, the wire was clamped down next to the glass slide. This insured motional stability and a means of electrical connection. The chromel wire was inserted from the right. It had already been clamped down onto an arm extending from a worm gear. This allowed the chromel wire to be moved in extremely small increments to facilitate wire alignment. Thus one hand was used to control the manipulator while the other turned the worm gear to move the chromel wire into position. After the chromel wire was butted against the constantan wire, the ends were aligned using the manipulator with the aid of a 20x microscope. At this point, the junction resistance was measured to assure continuity. This capacitor was typically 9 to 10 ohms. To create the butt weld a 3.7 μf capacitor was discharged across the junction. This capacitor was in series with a variable resistor. This configuration allowed the capacitor to be charged to different voltages. A voltage of approximately 210 volts was first applied to weld the wires. If the junction appeared to have been formed properly, it was annealed by discharging the capacitor 20 times in 10 sec increments at a voltage of 120 volts. The junction resistance was once again measured and typically was about 7 ohms. The thermocouple was removed from the alignment stage and optically inspected from all sides using the microscope. Since the junction was difficult to locate with the unaided eye, a very small mark is made on both sides of the junction with blue machinists ink. To keep the ink bolus from catching on tissue, the bolus was smoothed with an alcohol saturated cotton swab. At this point, the thermocouple was ready for use.

Section 2.2.2 Thermocouple Response Acquisiton

Two separate data acquisition systems were employed to monitor the thermocouple response. The first system consisted of a Keithly microvoltmeter and an oscilloscope. The output of the thermocouple was connected to the microvoltmeter. Using the microvoltmeter, the stability of the response before heating could be examined and any d.c. bias nulled out. The signal was amplified by the Keithly with a gain of 10E05 and fed to the oscilloscope for visual inspection of the thermocouple response. This system was especially useful when beam plotting the transducer and permanent recordings of the response was not desired.

To obtain a permanent copy of the thermocouple response, a Hathaway oscillograph was used. The thermocouple signal was applied directly to the oscillograph which consisted of a sensitive galvanometer that deflects a light source that was shining on light sensitive paper. The sensitivity of this galvanometer is such that an input thermocouple response of 60 uV (a 1°C change in temperature) will produce a 1.28 cm deflection on the oscillograph paper. This paper was darkroom processed after all the data had been recorded. The recordings produced look like the curve in figure 4. To obtain a value for the initial time rate of change of temperature (dT/dt), in °C/sec from this instrument, the following formula is used;

$$\frac{dT}{dt} = \left(\frac{dT}{dE}\right) * \left(\frac{di}{dx}\right) * \left(R_{TH} + R_{GAL}\right) * (SLOPE) \qquad (10)$$

where (dT/dE) is the thermocouple sensitivity (°C/uV), (di/dx) is the galvanometer sensitivity (0.545 uA/cm), Rgal is the resistance of the galvanometer(43.5 ohms), Rth is the resistance measured across the thermocouple leads in ohms, and Slope (cm/sec) is the slope of the thermocouple response curve at at 0.5 sec. All of the data discussed in Chapter 4 was obtained using the oscillograph.

Section 2.3 The Irradiation Apparatus

Having now detailed the physical characteristics and theory of the ultrasonic source and probe, attention is now turned to the exposure system. This system consists of a 36 liter Plexiglas tank placed on a 3 axis programmable milling machine base (Bridgeport). The specimen/thermocouple support structure which was positioned opposite the transducer, was supported in the tank by a clamp extending from the back tank wall. The transducer was held in a fixed position relative to the tank and specimen structure by a clamp above the tank. A schematic of this exposure system is shown in figure 7.

The tank was filled with the ultrasonic propagation medium. Degassed distilled water was used in this experiment due to its extremely low acoustic attenuation, low cavitation probability, and limited ionization effects on thermocouple connections. In the bottom of the tank was a heating coil used to keep the water at a constant 37°C. At the end of the tank, behind the specimen structure was highly absorbing acoustic foam (SOAB) (B.F. Goodrich) to minimize standing wave effects. The position of the mill base was controlled by 3 separate Slo-Syn preset indexers, one for each axis of motion. Bidirectional increments of 0.001 in. to 9.999 in. could be selected using the indexer. The extent of motion was recorded by feedback from 3 optical encoders which slide over 3 staionary transparent glass graticules. The digital information obtained from the encoders was displayed on separate X,Y, and Z Digi-Point digital readouts. The orientation of these coordinate axes, which will be of great importance in the following chapters, is also shown in fig 7.

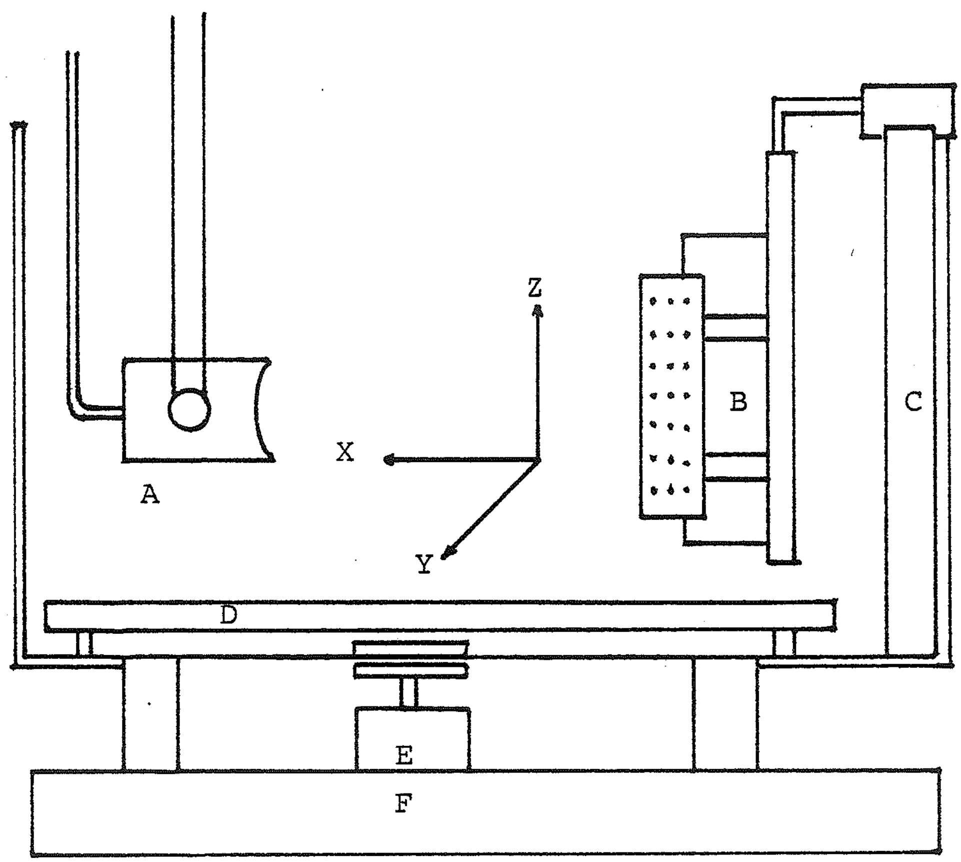

Figure 7. Schematic of exposure apparatus with coordinate system A) transducer B) specimen structure, C) SOAB backing, D) in-tank heater, E) magnetic stirrer, F) 3 position milling base

A device which could uniformly move a thermocouple through the body was essential. Already existing was a mouse mount which secured the mouse for irradiation. It was decided to couple a suprastructure with this mount to facilitate thermocouple movement. There were a number of design aspects to be considered in the construction of this suprastructure, such as: 1) the insertion and connection of the thermocouples require minimal thermocouple movement because of their fragility; 2) many thermocouple alignment positions to probe different tissues and account for individual mouse size variability; 3) and indicator of the amount of penetration of the thermocouple to correlate the tissue probed with its thermocouple response curve; 4) bidirectional movement for replication of previous responses; 5) time and effort preparing the suprastructure should be minimal; 6) ease of construction.

After several designs, consultations, and a few substitutions, the final design was arrived at. The complete system is shown is figure 8 and the detailed schematic of the suprastructure is shown in figure 9. The material selected for the building of the suprastructure was Plexiglas because of its availability, workability, and cost effectiveness. Stainless steel was used for the metal parts, due to its ability to resist the effects of saline solutions. The use

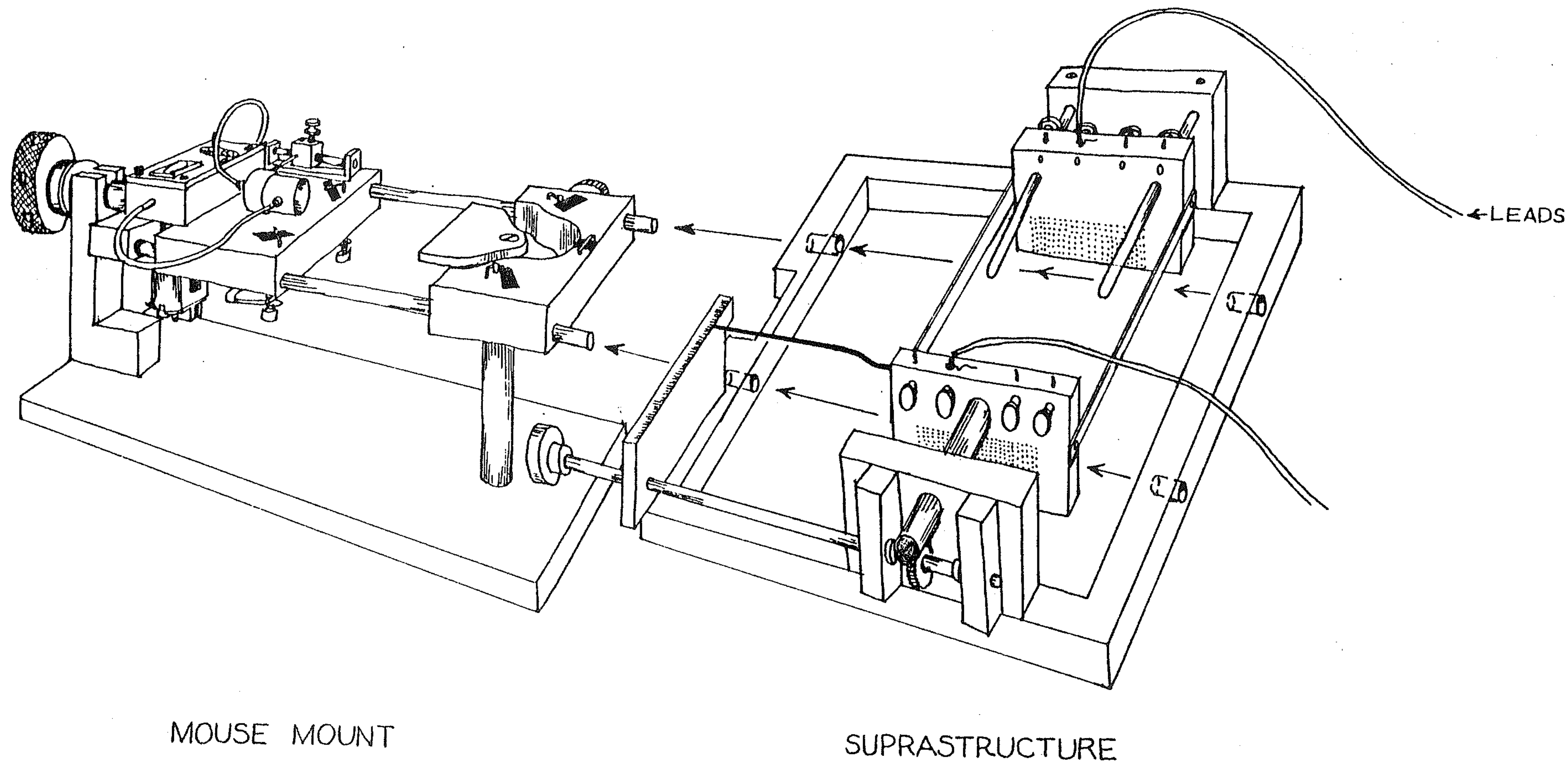

Figure 8. Complete specimen structure

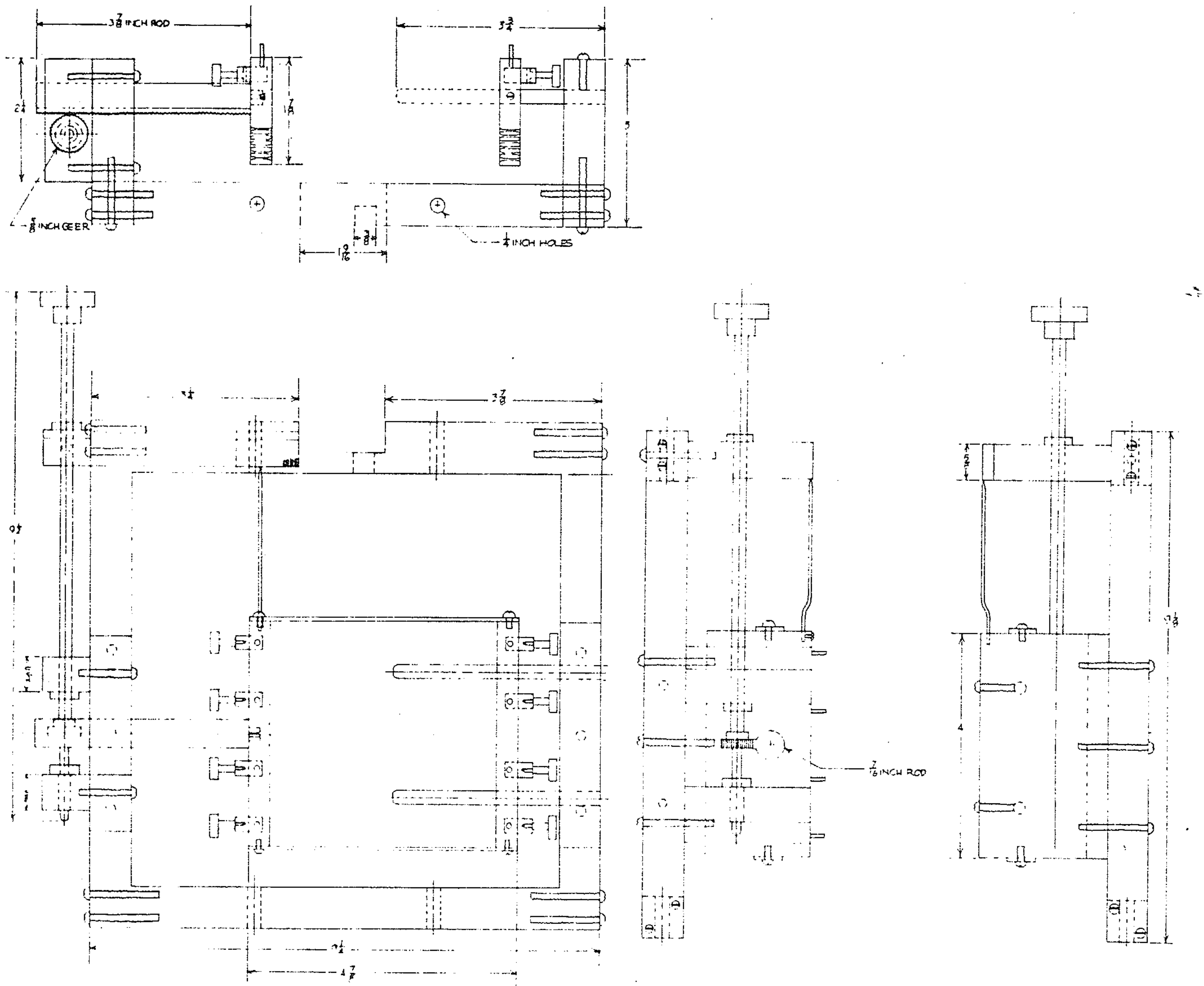

Figure 9. Detailed schematic of suprastructure

of the specimen/thermocouple structure in the experimental procedure is detailed in the following chapter.

CHAPTER 3

THE EXPERIMENTAL PROCEDURE

This chapter details the experimental procedures used to obtain the data necessary to compose an ultrasonic dosimetric model. This procedure was comprised of three distinct parts. First, the acoustic field was characterized without the specimen in place. Next, the specimen was prepared and irradiated. Finally, the tissue type of each irradiation site was determined through histological preparation of the specimen.

Section 3.1 Acoustic Field Characterization

The acoustic field produced by the transducer was considered to be a free field. A free field is characterized by plane progressive wave fronts of lateral extent where any standing wave effects are nonexistent. To construct a representation of this acoustic field, cross-sections of the field at various axial coordinates were obtained. These cross-sections are composed of point samples of some acoustic parameter taken at specific points in the plane. Since intensity was the field parameter to be used in the *in vivo* absorption measurements (equation 9), it was logical to use intensity as the parameter to be sampled in the free field characterization. To obtain these intensity samples, a transient thermoelectric probe was used for the precise calibration of the ultrasonic field. This technique has been used for many years in the Bioacoustics Research Lab and has been thoroughly described in the literature both for free field intensity determination (Dunn and Fry, 1957) and for in situ ultrasonic absorption and intensity determination (Goss et al, 1979). For the free field detection of ultrasonic intensity, the probe consisted of a 0.5 mil lap soldered thermocouple imbedded in a fluid medium which was contained by two 76 μm thick polyethylene acoustic windows and a steel housing. Two views of this probe are shown in figure 10. Silicon 710 (Dow Corning) was used as the embedding medium because its density and acoustic velocity are very similar to those of water and because its absorption coefficient is well known (Goss et al,1977). Thus, the incident sound energy reflected was small and the temperature change could be related to intensity by using equation 9. This probe was a phase insensitive device and no information about wave shapes could be determined using it.

The intensity at any point in the field can be calculated by using the temporal temperature response of the thermocouple probe, the known absorption coefficient and ρC of Silicon 710, and the use of equation 9. If this absorption coefficient and ρC are assumed always constant

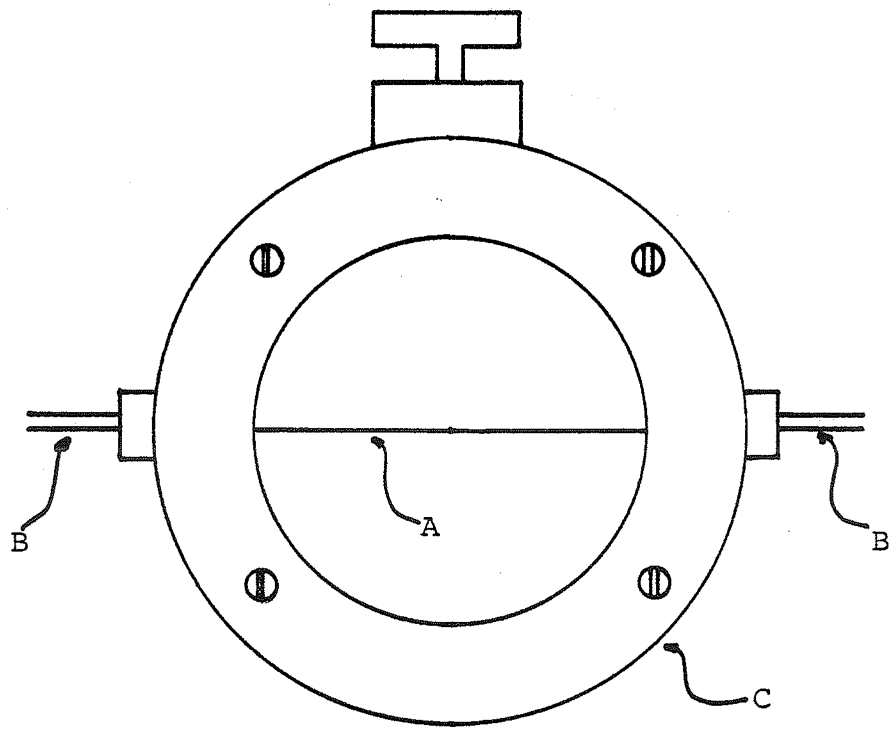

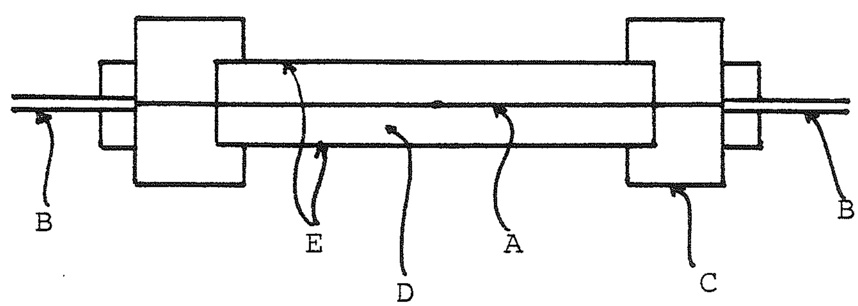

Figure 10. Schematic of calibrator
A) thermocouple wire, B) calibrator leads, C) steel housing, D) imbedding fluid, E) polyethylene acoustic windows

with respect to temperature and the time frame of this experiment, intensity and time rate of change of temperature are directly proportional. Furthermore, the magnitude of the net temperature change is also directly related to the time rate of change of temperature. An examination of the net temperature rise at the end of the acoustic disturbance will directly yield information about the magnitude of the relative intensity. If the calibrator is moved on a line perpendicular to the focal axis, a relative intensity beam pattern may be plotted. The calibrator is then moved to a line that is also perpendicular to the focal axis, but orthogonal to the first line. Another beam plot is done. These two beam plots are combined to create a field cross-section. This process is repeated at succesive axial positions to obtain a three dimensional representation of the acoustic field.

The experimental set-up for the free field characterization was much the same as that in figure 7. In place of the specimen structure, the calibrator was used. The tank was filled with 36 liters of degassed distilled water. A syphoning process was used to reduce to introduction of air into the solution. The tank heater was set for 37 $^{\circ}$C. To aid in heating the solution, two other heaters were placed in the tank. A magnetic stirrer at the bottom of the tank mixed the water. The transducer was positioned in the tank and its cable connector was attached to the driving network. The driving system was then switched on to allow proper warm-up. A 7.5 cm long pointer was placed on the front of the transducer housing. Since there is a 3 mm separation between the transducer face and the housing, the tip of this pointer is 7.8 cm away form the transducer face. This pointer tip indicates the region of maximal axial intensity (focal region) as determined by previous field calibrations. After the water temperature had reached 37 C, the calibrator was placed in the tank parallel to the transducer face so that the thermocouple wire was normal to the focal axis and parallel to the bottom of the tank. This placement was done by visual inspection. The calibrator was moved foward until the thermocouple junction was as close as possible to the transducer pointer tip. Care was taken to not puncture the acoustic window. This particular transducer/calibrator orientation was assigned the origin coordinate (0,0,0). Using the coordinate system of figure 7, the thermocouple was coincident with the Y axis, the focal axis was the X axis, and the thermocouple junction was at the origin coordinate. All subsequent measurements were referenced to this point. In this calibration procedure the probe was moved with respect to a stationary transducer. The calibrator was backed away from the transducer to allow the pointer to be removed. The calibrator was then retuned to the origin.

The variable capacitor was set so as to produce a maximal axial intensity of 2.44 W/cm**2. This intensity produced a suitable thermocouple output for beam plotting. The pulse length was chosen to be 0.3 seconds with a carrier frequency of 0.98 MHz. In this procedure, the thermocouple response was examined using the microvoltmeter/oscilloscope system.

The first field cross-section was obtained by moving the calibrator through the field in the YZ plane along the Y axis and then along the Z axis. The two relative intensity beam profiles obtained by this process are shown in figure 11. The actual shape of the focal region is slightly elliptical rather than circular. The transverse diameter in the Y direction is 5.0 mm, while that in the Z direction is Dt=4.0mm.

A series of field cross-sections were examined, using the same process as above, by incrementing X each time. The beam plots done in the diverging part of the field (-X) show a broadening of the intensity profile with a corresponding drop in the maximal axial intensity. The beam plots in the converging part of the field (+X) become very complicated and difficult to describe. These effects can be explained using the piston source theory discussed previously. The measured relative axial intensities are plotted in figure 12. It

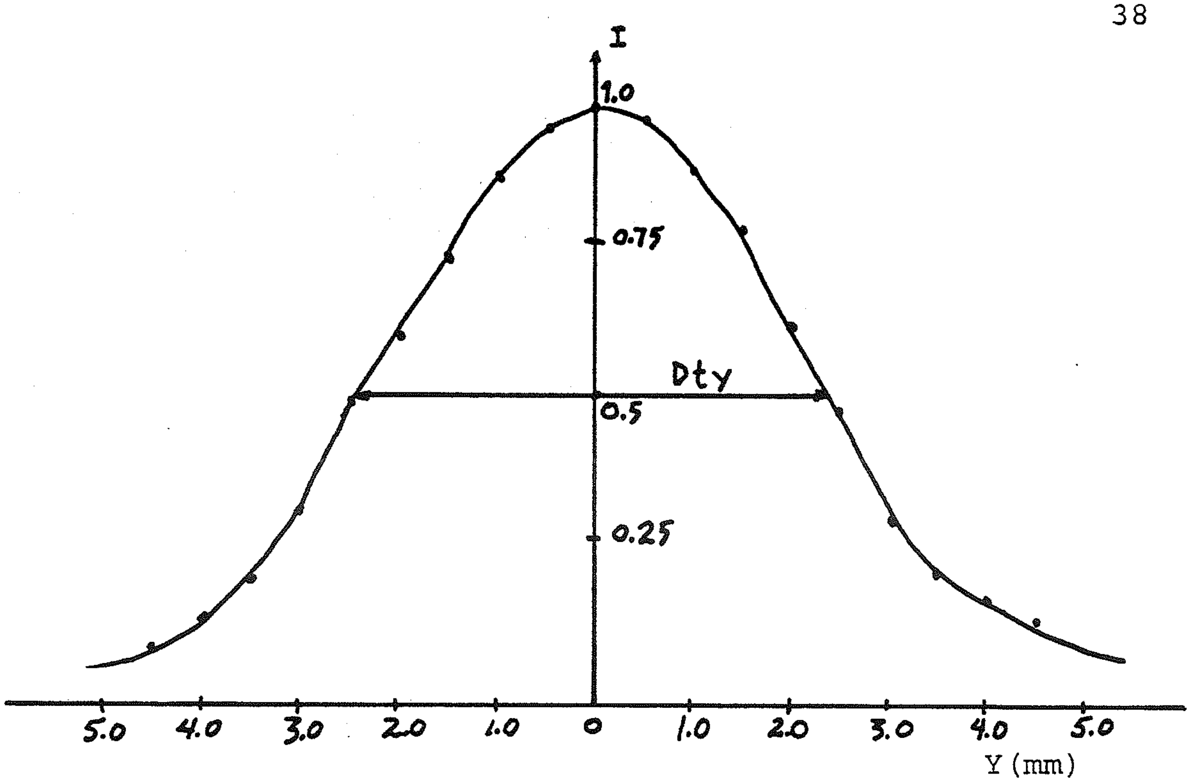

A) Beam plot along Y axis

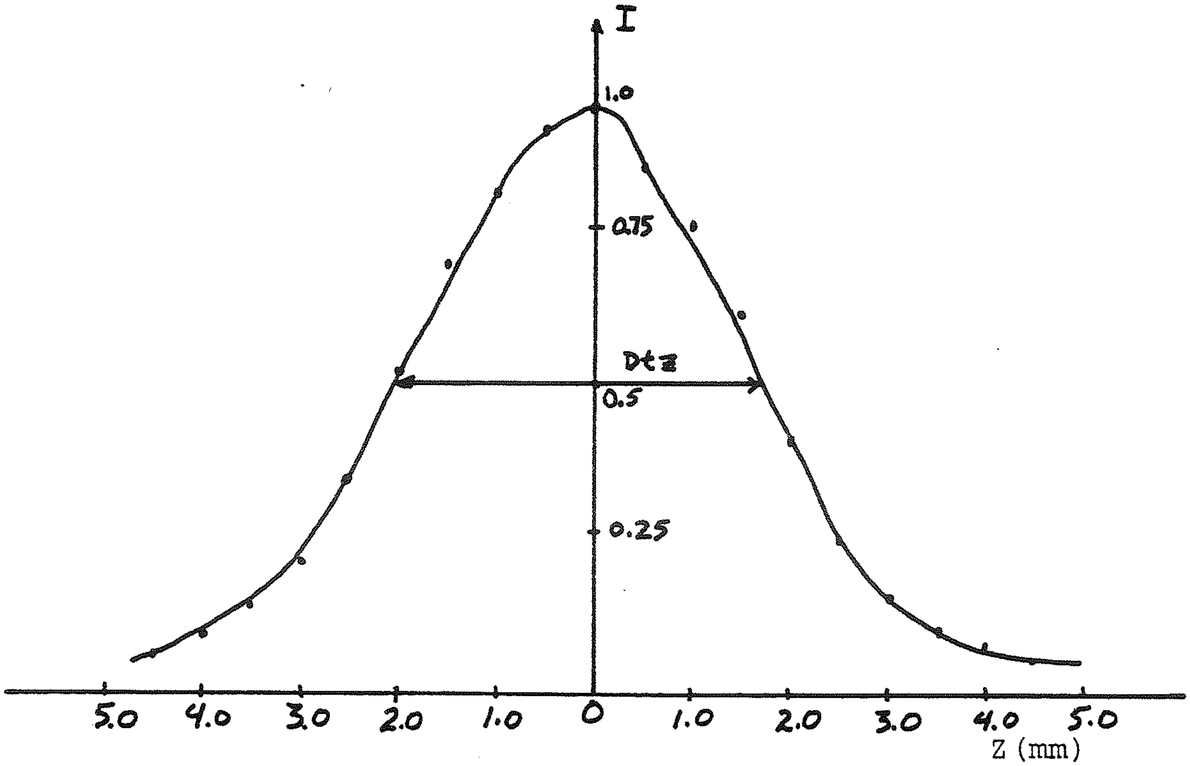

B) Beam plot along Z axis

Figure 11. Beam plots obtained along Y and Z axes

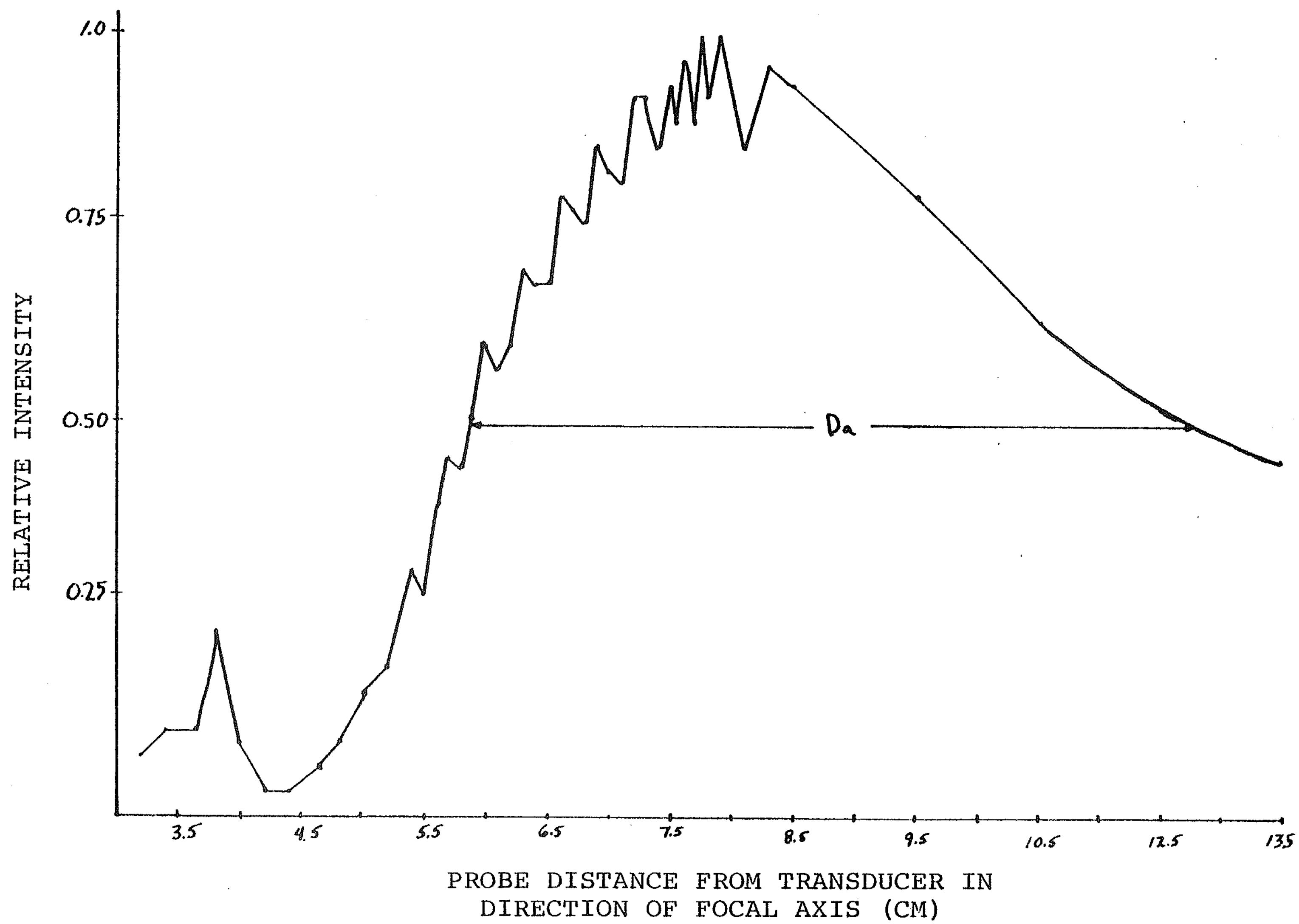

Figure 12. Relative intensity along focal axis

appears the true focal point of this transducer is indeed 7.8 cm from the face of the transducer.

The focal length determination from figure 12 was somewhat difficult due to the "ripple". The most likely cause of this was standing waves created by reflections from the SOAB tank backing. The true period of this standing wave was difficult to determine because the sampling increments used were integer multiples of $\lambda/3$. The true standing wave pattern would be seen if sampling increments of one tenth the wavelength were used.

It was obvious that characterizing an acoustic field in this manner was a tedious process. Fortunately, frequent calibrations over the life of this transducer has shown the output to be quite stable with respect to time. Therefore this procedure does not have to be repeated often. The important field characteristics and dimensions have been determined. The interactions between this field and a specimen may now be investigated.

Section 3.2 Specimen Preparation and Irradiation

In this procedure the specimens to be irradiated were LAF1/J mice obtained from Jackson Labs in Bar Harbor, Maine. Each specimen was administered a diet consisting of only water for the three days prior to the irradiation date. This starvation condition was necessary to minimize intestinal gas and fecal matter. If gas were to be present when the mouse was irradiated, the *in vivo* field would be drastically altered. The fecal matter is extremely heterogeneous, and thus it would be difficult to correlate the actual material at the irradiation site with the thermocouple response. Most of the body fat was also eliminated by this procedure. This is not desirable if body fat is to be a tissue of interest.

Prior to the experiment, the tissues to be irradiated were chosen. The thermocouple path through these tissues was limited by three constraints. They were: 1) the tissues to be irradiated had to spatially occur in a straight line; 2) the specimen structure allowed only a limited number of thermocouple wire orientations; 3) the irradiation procedure demanded that when the mouse was placed in the tank, the thermocouple wire should have been coincident with the Y axis (see Section 3.2.1). The second constraint can be alleviated through redesign of the specimen structure (Vaughn, 1980).

The experimental set-up is shown in figure 7. The preliminary experimental procedure was the same as in Section 3.1. As the water was coming up to temperature, the mouse was prepared. The starved mouse was placed in a glass chamber containing Metofane (Pittman-Moore Washington

Crossing, NJ) or chloroform. The mouse was removed when there was no pedal response. The anesthetic dosage administered was lethal. This was a necessary part of the experimental procedure for a number of reasons. During irradiation the thermocouple response would be adversely effected by the respiration and other body movements of an anesthesized mouse. Secondly, the mouse orientation in the specimen structure in a number of irradiations would drown the mouse. Finally, the specimen would have to be sacrificed immediately after the irradiation in any event, to facilitate the histological preparation. Fortunately,it has been shown that in the three hours required to perform the irradiation procedure, tissue characteristics do not change drastically (Bamber et al, 1977). The results obtained from the specimen tissues should yield an accurate representation of fresh, if not living tissues.

After anesthetization, the mouse was prepared for placement in the specimen structure. First, all the fur was removed from the area between the fore limbs and the hind limbs on all sides of the body. Electric clippers were used to remove most of the fur, followed by an application of commercial cream depilatory to remove all remaining stubble. After 15 minutes, the depilatory was rinsed off and the mouse was dipped in a water/shampoo solution. This left a slick film on the mouse body which discourged bubble adherence.

To place the thermocouple wire in the tissues of interest, a 22 gauge 1.5 inch hypodermic needle was inserted into the mouse along the thermocouple path decided upon previously. The thermoucouple was then carefully threaded through the hypodermic needle, and was held while the needle and was removed from the body. This process left the thermocouple wire in the body on a path through the tissues of interest.

The mouse was then secured in the support structure. The orientation of the mouse depended on which side the acoustic energy was to be incident. In subjects numbered 1 to 32 and 51 to 52, the mouse was placed head up, with the ventral side facing the transducer. In subjects 33 to 50, the mouse was placed head down, with the dorsal side facing the transducer. After the mouse was properly secured, the thermocouple ends were threaded through the support holes. These two holes were chosen so that the thermocouple wire would slide through the mouse parallel to the bottom and back of the tank. In otherwords, there should have been no deviation of the thermocouple path in the X or Z coordinates. The thermocouple was pulled through the mouse until the junction appeared at the skin perforation at the mouse's right side. The blue ink marks were utilized to identify the exact location of the junction. The thermocouple wire ends were secured in the brass external lead connectors. This was done in such a manner as to tauten the wire but to leave the junction position undisturbed. The external thermocouple leads were attached to the brass connectors. The resistance across these leads was measured. This resistance value was used for Rth in equation 10. The tiny perforations where the thermocouple entered and exited the skin were stained dark green with an astringent dye. The midway skin point between these two perforations was also stained. These markings were used as an aid in the histological preparation. The thermocouple junction was then moved from its present location through the mouse to the other skin perforation on the left side. The distance the thermocouple junction traveled from the right side skin perforation to the left side skin perforation was measured using a vernier/pointer configuration. This path length was recorded for use as a comparative standard in the irradiation procedure. The thermocouple was then returned to the skin perforation on the right side for later alignment in the tank. Figure 13 shows a specimen prepared for irradiation.

Section 3.2.1 The Coordinate System and Alignment Procedure

The specimen/thermocouple structure was placed in the tank opposite the transducer. The transducer was brought up to the mouse so that the pointer tip was touching the thermocouple junction at the right side perforation. This

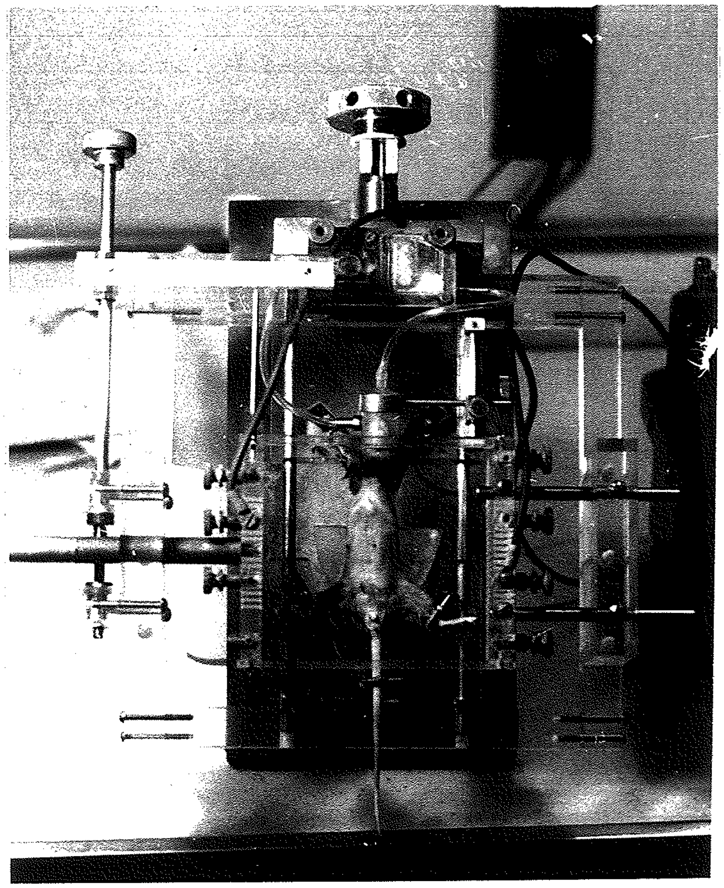

Figure 13. Prepared specimen secured for irradiation

specimen/transducer/thermocouple junction orientation was assigned the origin coordinate of (0,0,0) as seen in figure 14. Recall this tip indicated the location of the focal region. In this procedure the location of the focal region was used to report the position of the transducer. This was done in order to directly obtain the coordinates of the irradiation site within the specimen. Therefore, the relationship between the "*in situ* intensity" and thermocouple response could be examined in the same manner as Section 3.1.

At the origin the thermocouple was coincident with the Y axis, the focal axis was the X axis and the thermocouple junction was at the intersection. The specimen was stationary in space with respect to the coordinate system. The thermocouple junction moved only along the Y axis, and thus the junction positions were recorded in only one coordinate (Y). The focal region was moved in three dimensions and thus its coordinates were recorded as (X,Y,Z). Notice that both the thermocouple junction and focal region positions were recorded using the same coordinate system. Therefore, by simple inspection of the reported coordinate positions, the precise orientation between the thermocouple and focal region was known.

The length of the thermocouple path was measured again by moving the transducer to the left perforation. This new

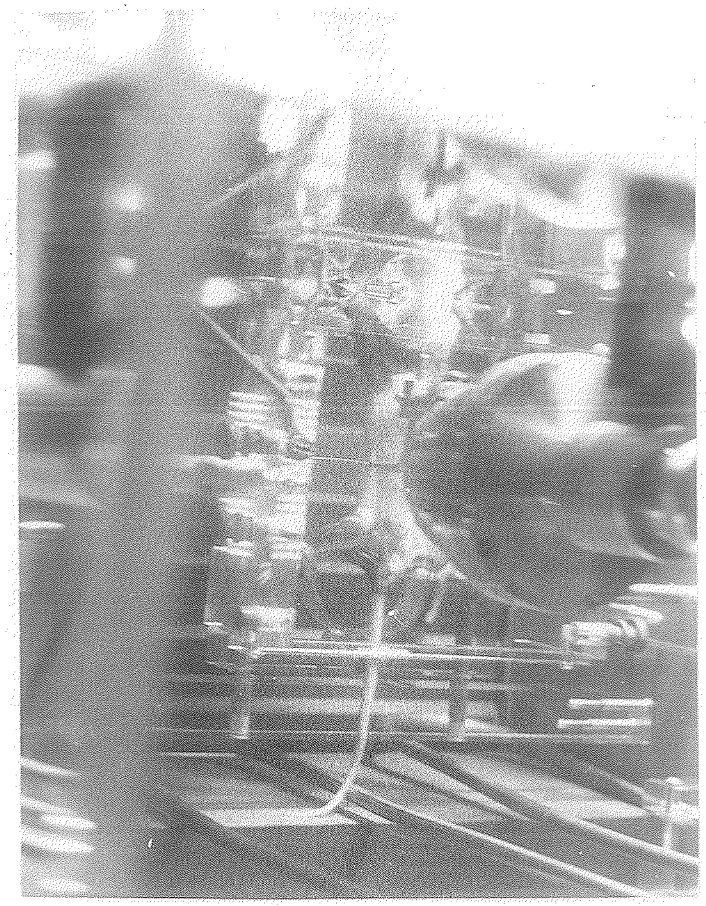

Figure 14. Specimen fixed in tank with transducer focal tip and thermocouple junction at position assigned (0,0,0)

transducer position should have read (0,+Y1,0) if the structure is properly aligned. The value of Y1 should have equalled the path length previously measured outside the tank. If the transducer were moved in the X or Z directions to place the focal tip on the left perforation, the specimen structure was realigned. Upon realignment the origin coordinate was reset. After any structural realignment was completed, the transducer tip was moved to the center marking. The transducer position then read (+X,+Y1/2,0). The X value was an indication of the thermocouple depth under the skin surface at this point. The transducer was backed away from the specimen and the pointer removed. The transducer was then moved back so that the focal region was again at the origin.

To insure that the thermocouple junction was aligned properly in the focal region, beam plots like those described in Section 3.1 were done. The origin though, was not a satisfactory thermocouple location to do a beam plot, as the skin/water interface often yielded some unusual results. The thermocouple and transducer were both moved 4.0 mm in the +Y direction to a different irradiation site. In this position adequate _in vivo_ beam plots were usually obtained. The criteria used for centering the junction in the focal region was attainment of the maximal relative intensity in both the Y and Z directions. It was intended that this location of maximal intensity would coincide with the alignment obtained with the pointer centering process, although this was not always the case. Upon inspection of the two beam plots done in the Y and Z directions, it occasionally was found that the thermocouple was not in the locus of maximal intensity. The transducer position was readjusted so the maximal relative intensity in both the Y and Z directions was obtained. The thermocouple and transducer were moved back 4.0 mm in the -Y direction. If the transducer had to be realigned, the origin coordinate was reset.

A number of important assumptions were made in this alignment process and were used throughout the experiment. They were: 1) the movements of the thermocouple and transducer were always in the increments desired; 2) the scale for the thermocouple movement and transducer movement readout were accurate; 3) the thermocouple did not slip in the specimen structure, nor did the encoders on the mill base; 4) the ultrasonic beam was not refracted at the skin/water interface which would redirect the maximal intensity off the focal axis; 5) the focal region was always centered on the focal axis.

Section 3.2.2 Irradiation Algorithms

Once the thermocouple and transducer were properly aligned, the irradiations were begun. There were a number of possible irradiation algorithms that could have been implemented. The transducer and thermocouple could be moved in a one-to-one correspondence in the Y direction. This would keep the focal region over the thermocouple at each irradiation site. Another approach would be to obtain beam plots at each thermocouple position by moving the transducer in its YZ plane. This algorithm might yield more information concerning beam permutations. The thermocouple might be incremented through a stationary field (a beam plot in the Y direction) , the transducer is then moved and the process is repeated. The algorithm used in this experiment was the former. One-to-one correspondence yielded data which was easy to obtain and analyze. The second and third algorithms described above were used on a small number of specimens, but only to supplement the one-to-one data. It must be realized that the second and third algorithms are tedious and very time consuming processes, but will be easier to implement with a more automated precedure (Vaughn, 1980).

The implementation of the one-to-one algorithm was straightfoward. Beginning with the origin coordinate, the site was irradiated with a one second ultrasonic pulse of sufficient intensity to produce a legible, permanent copy of the thermocouple response output on an oscillograph. The thermocouple and transducer were simultaneously moved one millimeter in the +Y direction. This new site was then irradiated using the same exposure conditions as the previous location. This process was continued until the junction exited the left side perforation. At each location the following data were recorded; 1) thermocouple position (Y), 2) focal region position (X,Y,Z); 3) pulse length; 4)value of the variable capacitor Cs; 5) observations of unusual thermocouple responses.

Occasionally, the number of thermocouple positions which were taken in one millimeter increments, yielded a distance which exceeded the thermocouple path length measured twice before. The source of this error stemmed from the thermocouple adhering to the tissues. Although the junction was designed for smooth passage, it still occasionally snagged on the tissues. This was especially true at locations where the thermocouple entered or exited the body. The junction would snag on the skin and pull it along for 2-3 mm. Obviously, this changed the tissue orientation from the normal position, a situation which more than likely happened internally to varying degrees as well. To alleviate this problem, the junction was moved back and forth rapidly to dislodge the tissue and return it to its original location. This may have resulted in slight tissue damage, although it was felt such tissue damage did not effect the results.

After the last thermocouple response was recorded, the oscillograph paper was developed. If legible traces were obtained, the mouse was prepared for the histological sectioning process.

Section 3.3 Histological Preparation of the Specimen

To fully make use of the thermocouple response data obtained by the procedure in Section 3.2, the tissues comprising the thermocouple path must by identified. A method to precisely and accurately describe the path of the thermocouple was devised (Wyneken and O'Brien,1980). This freeze-sectioning technique allows for both gross and semimicroscopic anatomical information to be obtained through thick sectioning.

Following the irradiation procedure, the specimen still contained in the structure was submerged in an ice bath. In order to maintain temperatures suitable for rapid freezing at approximately -10 C, 4-5 liters of a saturated salt solution (290 gm/l) were mixed with 3600 grams of crushed ice. The specimen structure was maintained in the same orientation in the ice bath as it was during the irradiation process. The specimen could be removed from the ice bath without distorting the internal organ locations after 10 minutes. The mouse was removed from the experimental holder, taking extra care not to disrupt the thermocouple wires, wrapped in plastic and placed in a -10°C freezer.

To obtain a section of the specimen, a specially constructed guillotine, cooled by a dry ice-90% alcohol bath, was used to cut rapidly through the animal along a dorsoventral plane (figure 15). Cuts were made on either side of the thermocouple wire yielding a cross-section piece approximately 8 mm thick. This section was packed in dry ice.

After cooling the freezing stage of a sliding arm microtome with a dry ice-90% alcohol bath, a paper collar was fitted around the 8 mm thick section on the stage and an ice base was built inside of the collar. This technique is similar to that of mounting a specimen on an object disk of a cryostat with an embedding medium which in this case is water, and the collar is required to contain the water prior to freezing. The cross-section piece was placed with its flatter surface down inside the collar. Care was taken to note which surfaces were cranial or caudal. Small amounts of water were added around the base and the entire collar was then packed in crushed dry ice, freezing the 8 mm thick specimen to the base. This configuration is shown in figure 16. Prior to sectioning the specimen, the paper collar was removed.

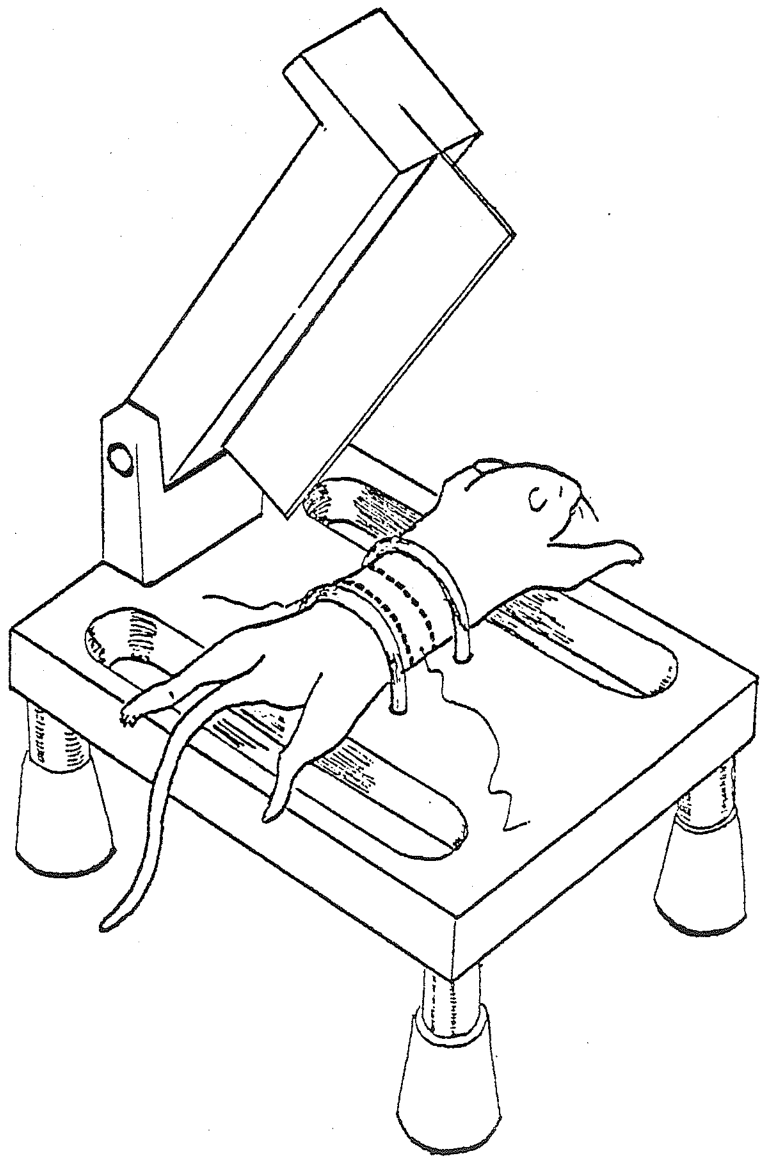

Figure 15. Specimen sectioning guillotine

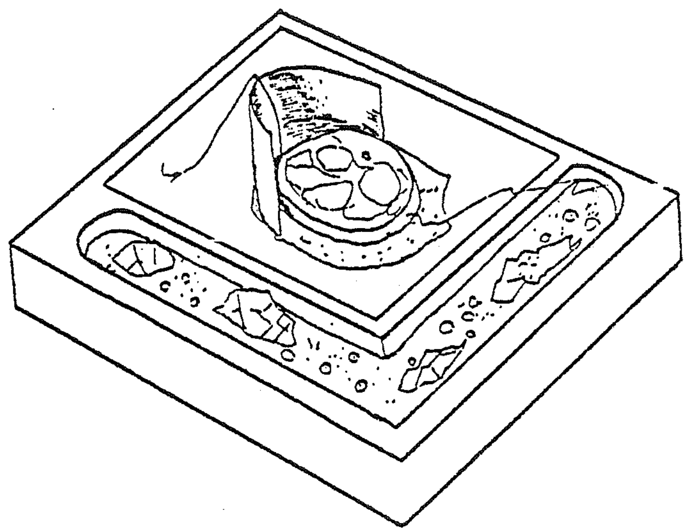

Figure 16. Specimen section freezing stage

The plane of section was determined using the entrance and exit skin perforations caused by the thermocouple wire and a third point determined by the position of the animal relative to the ultrasonic beam axis. These three spots had been stained dark green during the irradiation preparations to mark the plane of section.

Relatively thick serial sections (80 µm -120 µm) were made and mounted on gelatin coated slides. If these sections were to be saved, they were frozen or fixed using a treatment of absolute alcohol followed by flowing 0.75% celluloden solution in ether or alcohol, then 1 minute in 80% alcohol. Sections were removed until just before the level of the thermocouple was reached at which point the two ends of the thermocouple wire were attached to a six volt battery for approximately one minute to create a sear. The sear mark leaves a permanent visable record of the path of the thermocouple wire. The thermocouple wire was then removed and sectioning continued until the level of the sear was reached.

A scaled representation of the entire section at the level of the thermocouple was drawn with the aid of a Fowler Scale Magnifier equipped with a 10 mm grid reticule. All organs and tissues in this drawing were identified and labeled. The tissue type at each irradiation site was recorded, as well as the distance between the site and the irradiated skin surface in the direction of the focal axis. Furthermore, each interposing tissue type between the skin surface and irradiation site was identified and dimensioned. These interposing tissues were recorded in order of their spatial occurence along the focal axis for each irradiation site. Thus, the acoustic propagation path to each irradiation site was characterized. This information combined with the dosimetric data obtained in Section 3.2 can yield the spatial distribution of ultrasonic energy within the specimen.

CHAPTER 4

RESULTS AND OBSERVATIONS

In this chapter the data obtained from the irradiation and histological procedures described in Chapter 3 are collated and examined. The reasons for changes of the specimen orientation in the irradiation procedure over the course of the experiment are explained. A model to calculate the acoustic intensity at each irradiation site within the specimen is proposed. Using this calculated "*in situ* intensity" value, the absorption coefficient of the tissue at each site is determined and entered in to a dosimetric file with pertinent irradiation and histological data. All irradiation sites in this dosimetric file which have the same tissue type are grouped together. The absorption coefficient results for each tissue type are compared to literature values. Observations are made on this absorption coefficient data and improvements to the model are suggested.

Section 4.1 Discussion of the Experimental Procedure

During this experiment, 53 specimens were irradiated. The results from a number of these specimens were not utilized in the analysis because: 1) the thermocouple responses were not legible on the oscillograph paper; 2)the histological data were not obtained due to improper freezing or sectioning techniques; 3)a one-to-one correspondence did not exist between the number of irradiation sites exposed in the irradiation procedure and the number of sites determined histologically. This last reason was discussed in Section 3.2 and concerned the snagging of the thermocouple junction in tissues. If the thermocouple did pull tissues out of their normal orientation, then more irradiations sites would be recorded than expected. If the tissues then pulled free and returned to their original orientation before the specimen was frozen, then the histologist would find fewer irradiation sites than recorded in the irradiation procedure. Therefore, it would be subject to considerable error to correlate the thermocouple responses with the histological data.

The valid specimen data were classified into two categories. These categories were partitioned by the orientation of the mouse in the support structure during irradiation. As it turned out, there was no need to analyze the data separately by this classification. Although it is convenient to discuss the experimental procedures in this manner. The first category consisted of the specimens (numbered 17 to 32, 52 and 53) which were irradiated head up, ventral side facing the transducer. Within this group two different thermocouple paths were utilized. In specimens 17 to 20, 25, 29 to 32, 52 and 53, the thermocouple wire was inserted just under the abdominal skin surface. In specimens 21 to 28 the thermocouple wire was inserted through the intestinal and gut area. It was found in these specimens that when the thermocouple junction was in gas or fecal matter an atypical thermocouple response was produced. In figure 17 a thermocouple response received from an area in specimen 25 known to contain gas and fecal matter is contrasted to a typical thermocouple response. Notice that it is nearly impossible to define a linear region and obtain a satisfactory value for dT/dt from trace A.

Since the contents of the intestinal tract markedly effects acoustic wave propagation, the irradiation procedure was changed so as to avoid irradiating the intestinal tissues. Also, it was decided to probe a well characterized tissue. Kidney was chosen because of its accessability and known absorption and attenuation coefficients (Goss et al,1979). To avoid having the sound beam pass through intestinal organs before striking the kidneys, the mice were irradiated from the back. To accomplish this using the existing specimen structure, the mouse was placed head down, dorsal side facing the transducer. Specimens 33 to 44, 47, 50, and 51 were irradiated in this fashion and comprise the second category.

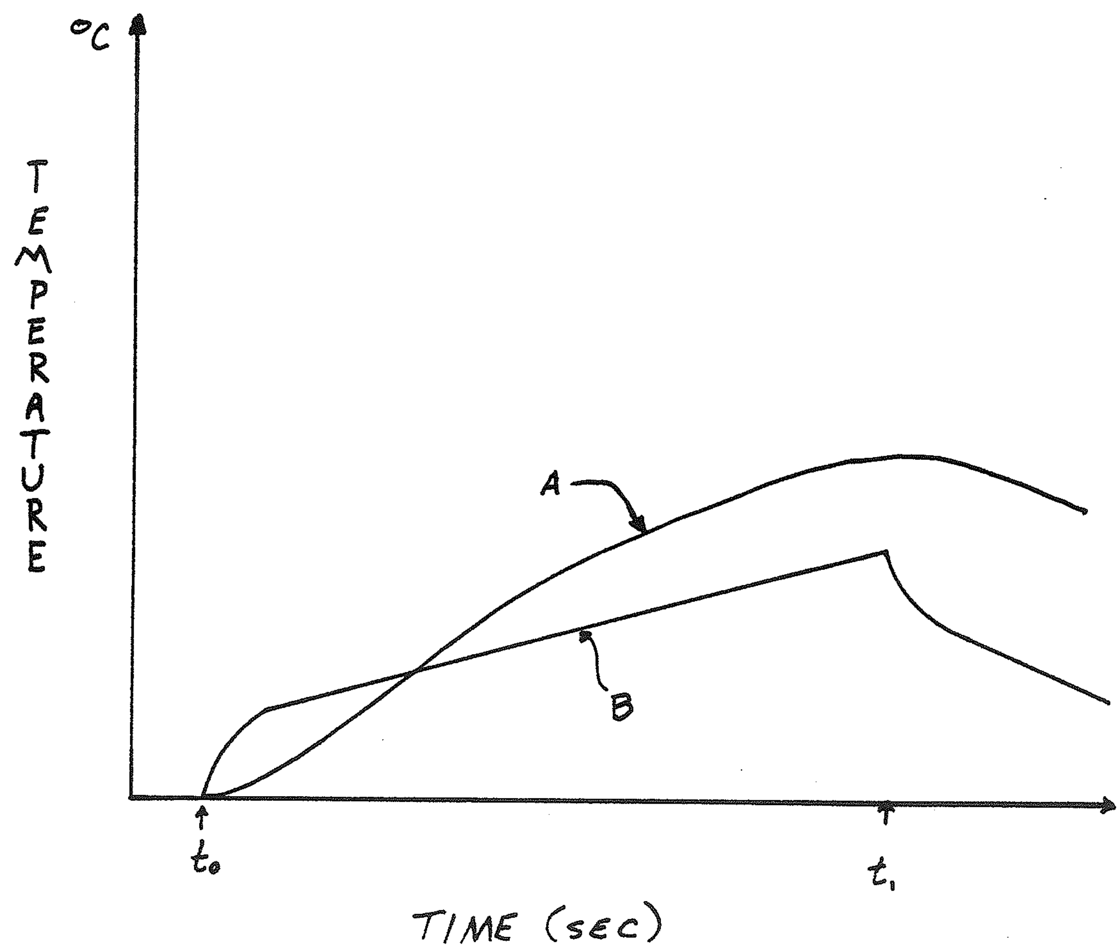

Figure 17. Comparison of an intestinal thermocouple response (A) to a typical response (B)

Section 4.2 The Irradiation Files

Because of the large amount of data and to facilitate data compilation and analysis, all irradiation and histological data were stored in an Interdata 7/32 minicomputer(Perkin-Elmer Oceanside, NJ). The experimental irradiation data file (DOSEXPR.DTA) was arranged to accomodate data from very complex dosimetric experimental procedures. Although the file has provisions for accepting data from specimens probed with multiple thermocouple wires, only one thermocouple wire was used in this study. The file was ordered by specimen number beginning with specimen 17. The data entered in this file for each irradiation site were: 1)specimen number; 2) thermocouple probe number; 3) coordinates of the focal region (inches); 4) shot number; 5) thermocouple junction position as recorded with the vernier scale on the specimen structure (mm); 6) time rate of change of temperature measured from the oscillograph (cm/sec); 7) net temperature rise at the end of the acoustic disturbance obtained from the oscillograph (cm); 8) value of the variable capacitor Cs.

Some of these data were not entered in its most useful form for dosimetric analysis. A fortran program (DOSEXPR.FTN) was written which: 1) converted the focal region coordinates from inches to millimeters 2) normalized the thermocouple position to a Y axis value with respect to the coordinate system (mm); 3) converted the dT/dt and net temperature rise values to °C/sec and °C respectively using equation 10; 4) calculated the acoustic intensity produced by the transducer using the Cs value and equations 4 and 5; 5) create a new file (DOSEXPC.DTA) to store this converted data and items 1, 2, and 4 from DOSEXPR.DTA. A final DOSEXPC.DTA file specimen entry is shown in Appendix A.

Section 4.3 The Histological Data File

The histological data file (DOSHIS.DTA) was set-up in the same form as the DOSEXPC.DTA file to simplify the combination of the two files. The information recorded for each irradiation site in a specimen were: 1) specimen number; 2)thermocouple number; 3)coordinate of the thermocouple junction position with respect to the specimen (mm); 4) thermocouple depth below the skin surface in the direction of the focal axis (mm); 5) tissue identification code; 6) interposing tissues. This interposing tissue entry consisted of a 4X2 array. Each interposing tissue and its depth were recorded in order of their occurence in relation to the irradiated skin surface. Occasionally, there were more than four interposing tissues between the irradiation site and the skin surface. In this case, 999 was placed in the specimen number column of the next line to denote a continuation of the line before. The remaining interposing tissues and their thicknesses were entered on this line.

To facilitate tissue type data entry, a three letter code was devised for each tissue encountered in this experiment. This coding system is listed in table 1. Provisions were made to describe different portions of an organ. In some cases, the first 2 letters of the code identified the organ and the third letter denoted a particular part of that organ. For example, in the case of kidney there were codes for the cortex (KIC), medulla (KIM), surface (KIS), and kidney in general (KIG). KIG was used when a particular part of the kidney could not be distinguished. Furthermore, the coding system was extended to cover the case of when the thermocouple junction was located in an interface between two different tissues. The first letter of this interface code was the first letter of the tissue code through which the thermocouple junction had just passed. The second letter of the code was a J to denote a tissue/tissue junction. The third letter of the interface code was the first letter of the tissue code through which the thermocouple junction will pass next. For example, if the thermocouple junction was located in the kidney/liver interface, the tissue code would be KJV. Using the orientation of the scaled drawing (see Section 3.3) done from the histological specimen section, this code reads from left

Table 1: TISSUE CODES FOR THE HISTOLOGY FILE DOSHIS.DTA

ADP-FAT
BLO-BLOOD
BVV-BLOOD VESSEL
CNT-CONNECTIVE TISSUE
CRU-FECAL MATERIAL
DER-SKIN
FAS-FASCIA
GUG-STOMACH GENERAL
GUL-STOMACH LUMEN
GUS-STOMACH SURFACE
KIC-KIDNEY CORTEX
KIG-KIDNEY GENERAL
KIM-KIDNEY MEDULLA
KIS-KIDNEY SURFACE
LCG-CAECUM GENERAL
LCL-CAECUM LUMEN
LCS-CAECUM SURFACE
LIG-LARGE INTESTINE GENERAL
LIL-LARGE INTESTINE LUMEN
LIS-LARGE INTESTINE SURFACE
MMA-ABDOMINAL MUSCLE/SUBCUTANEOUS MUSCLE
MMB-BACK MUSCLE
NSP-SPINAL COLUMN
PLC-SPLEEN CORTEX
PLG-SPLEEN GENERAL
PLS-SPLEEN SURFACE
SIG-SMALL INTESTINE GENERAL
SIL-SMALL INTESTINE LUMEN
SIS-SMALL INTESTINE SURFACE
VEC-LIVER INTERIOR
VEG-LIVER GENERAL
VES-LIVER SURFACE
WAT-WATER

FOR INTERFACES, USE J TRANSPOSED BETWEEN THE FIRST LETTER OF THE TISSUE CODES, GOING FROM LEFT TO RIGHT.
EXAMPLE; LIVER/KIDNEY INTERFACE IS VJK.

to right. A specimen entry from the DOSHIS.DTA file is presented in Appendix B.

Section 4.3 The Dosimetric Model

To determine the absorption coefficient of a tissue using a thermocouple probe, the acoustic intensity at that location must be known. In this experiment only the free field intensity is known. An iterative model was developed to calculate the "*in situ* intensity" knowing this free field intensity produced by the transducer and the interposing tissues.

The basis of this model is the theory of sound transmission through multiple layered media. This transmission theory is explained in a number of texts (Kinsler and Frey, 1962). In this case the layered media are the interposing tissues. To use the multiple layered media theory to model the interposing tissues a number of assumptions were made. They are: 1) all tissue boundries were normal to the direction of sound propagation; 2) all wave fronts were plane progressive; 3) there was no mode conversion; 4) the attenuation coefficient and characteristic acoustic impedance were spatially constant for each layer; 5) there were no standing wave effects; 6) all wave phenomena were of infinitesimal amplitude and linear. Once these assumptions were made equations to calculate the "*in situ* intensity" could be formulated from the multiple tissue layer model.

As a plane progressive acoustic wave propagates through a medium which is lossy (tissue), the intensity decreases exponentially. The intensity at any point within the medium Ix, is given by;

$$I_x = I_o \exp(-2Ax) \qquad (11)$$

where Io is the original incident intensity (W/cm**2), A is the attenuation coefficient of the medium (Np/cm), and X is the depth of acoustic penetration (cm). When this acoustic wave impinges upon a boundary with a contiguous second medium, a reflected wave is generated in the first medium, and a transmitted wave is generated in the second medium. The fractional energy transmitted into the second medium is given by the sound power transmission coefficient αt;

$$\alpha t = \frac{4 Z_1 * Z_2}{(Z_1 + Z_2)^2} \qquad (12)$$

where Z1 and Z2 are the characteristic acoustic impedances of mediums 1 and 2 respectively. To find the intensity at an *in vivo* point P within the tissue of interest, where there are intervening layers of tissue between the point P and the skin surface, an iterative process using equations 11 and 12 may be used. This process is expressed numerically as;

$$I_s = I_o \exp\left(-\sum_{n=1}^{K} 2A_n X_n\right) * \prod_{n=1}^{K} dt_n \qquad (13)$$

where Is is the "*in situ* intensity" (W/cm**2), Io is the value of the free field incident intensity (W/cm**2), and K is the number of tissue boundries. In expressing equation 13 in this manner, it is assumed the degassed water is lossless.

To apply equation 13 to the data files, the attenuation coefficient and characteristic acoustic impedance of each interposing tissue must be known. A compilation of the literature values of these parameters for each interposing tissue is shown in Table 2. The values which are asterisked denote them to be approximated. These approximations were made from knowledge of the tissue constituents. Once the "*in situ* intensity" is calculated, the irradiated tissue absorption coefficient may be determined using equation 9. The value used for C in this equation is 3.77 J/°Ccm**3 (Goss et al,1977).

Section 4.4 The Dosimetric File

To calculate the absorption coefficient at each irradiation site a fortran program (DOS.FTN) was written

TABLE 2: COMPILATION OF CHARACTERISTIC TISSUE PARAMETERS TO BE USED IN EQUATIONS 11 AND 13 (GOSS AND JOHNSTON, 1978)

TISSUE CODE	TISSUE TYPE	VELOCITY (m/s)	DENSITY (g/cm)	IMPEDANCE (x10⁶ Rayls)	ATTENUATION COEFFICIENT Np/cm
ADP	Fat	1467	0.95	1.39	0.07
BLO	Blood	1566	1.042	1..63	0.02
BVV	Blood Vessel	1590		1.82	0.17
CNT	Connective Tissue	1625	1.08	1.75	0.35
CRU	Fecal Material			1.40*	0.40
DER	Skin	1720	1.1	1.89	0.24
FAS	Fascia	1600	1.05	1.60*	0.18*
GU-	Stomach			1.60*	0.07*
KI-	Kidney	1566	1.055	1.64	0.12
LC-	Caecum			1.60*	0.07*
LI-	Large Intestine			1.60	0.07*
MMA	Abdominal Muscle	1566	1.058	1.66	0.15
MMB	Back Muscle	1566	1.058	1.66	0.15
NSP	Spinal Bone	3445	1.82	7.8	1.6
	Spinal Cord	1615	1.03	1.66	0.25
PL-	Spleen	1567	1.059	1.67	0.009
SI-	Small Intestine			1.60*	0.07*
VE	Liver	1578	1.055	1.66	0.10
WAT	Water	1500	1.00	1.5	0.0

which combined the DOSEXPC.DTA and DOSHIS.DTA data files. This program calculated the "*in situ* intensity" and absorption coefficient using equations 8, 12 and 13 , and the experimental data for each irradiation site. A dosimetric file (DOS.DTA) was created which contained the data believed to be the most useful for the dosimetric analysis employed herein. The entries in this file were: 1) the specimen number; 2) thermocouple number; 3) thermocouple junction coordinates with respect to the specimen (mm); 4) tissue code; 5) thermocouple depth below the skin surface in the direction of the focal axis (mm); 6) time rate of change of temperature (°C/sec); 7) "*in situ* intensity (W/cm**2) 8) tissue absorption coefficient (Np/cm) at 1 MHz. A specimen entry from the DOS.DTA file is shown in Appendix C.

Section 4.5 Data Analysis

The data contained in the DOS.DTA file can be analyzed on two levels. On the tissue level, all irradiation sites of the same tissue type can be grouped together and their calculated absorption coefficients ( ) compared. It was felt that the assumptions upon which the dosimetric model was based could more easily be substantiated by examining the s at each irradiation site. On the specimen level, the relationships between irradiation sites within a particular specimen can be examined simultaneously. Useful information can be obtained by examining data on this level, especially in determining the energy absorbed by the specimen and the interaction of the acoustic field within the specimen. It is the intent of this section to examine the data on both levels and suggest improvements to the dosimetric model.

To facilitate the examination of the s on the tissue level, the DOS.DTA file was partitioned by tissue type. The results of this partitioning process are shown in tabular form in Appendix D. Presented on the first page of this appendix is the description of each of the columns in this table. Notice that not only are the tissues grouped with those of the same tissue code, but also with any pertinent tissue/tissue interfaces. For example, the skin group not only contains the irradiation sites which were skin (DER), but also contains the skin/muscle interfaces (MJD,DJM) and skin/water interfaces (WJD,DJW). These interfaces were included to acount for histological irradiation site determination inaccuracies of ± 0.5 mm. It was possible that the thermocouple junction may have been in the tissue of interest rather than in the interface.

In Appendix D, two tissues types, kidney and muscle, have large data bases. These two tissue groups were more closely examined to assess the practicability of the dosimetric model. The mean and standard deviation were calculated for the absorption coefficients of the two tissue groups. Recall that all the absorption coefficients calculated in this study were obtained using a 76 um thermocouple wire. When irradiated, this wire size will produce viscous heating effects which contribute to the heating response throughout the duration of the acoustic disturbance. Therefore, the measured time rate of change of temperature will be higher than the rate of change without the wire in place. Goss et al (1977) examined the errors associated with the viscous heating contribution at 0.5 MHz and presented a plot of theoretical error vs. true absorption coefficient. The 76 μm thermocouple line on this plot was used as a approximation of the error produced by the viscous heating at 1 MHz. Viscous heating is less dependent upon frequency than is the bulk heating due to absorption resulting in smaller errors due to this effect at higher frequencies. Thus, the error approximations taken from the Goss paper might be termed "worst case". Taking this viscous heating error into account reduces the mean absorption coefficient values by about 8%. The mean, standard deviation, "corrected" mean, and literature values for kidney and muscle are presented in Table 3. The kidney literature absorptin coefficient was measured using a 13 μm thermocouple junction (Goss et al,1979). A literature value for the muscle absorption coefficient did not exist at the writing of

Table 3: Summary of calculations on kidney and muscle absorption coefficient values.

Tissue Code	# of Irradiation Sites	Mean	Standard Deviation	"Corrected" Mean	Literature Value
KIC	67	0.0453	0.0274	0.0423	0.030
KIM	27	0.0550	0.0490	0.0520	"
KIG KIS	54	0.0510	0.0213	0.0475	"
HMA	73	0.0380	0.0228	0.0355	0.045
HMB	11	0.0315	0.0174	0.0283	"
HMB (under spine)	11	0.4342	0.4248	0.4342	"

this thesis. Goss et al (1979) reported the existance of a threefold difference between the attenuation and absorption coefficients for most soft tissues. Using this relationship and a value for the attenuation coefficient of 0.15 NP/cm (Table 2), the absorption coefficient for muscle is assumed to be 0.045 Np/cm. This is the literature value presented in Table 3.

The kidney data was inspected on the tissue level to detect flaws in the dosimetric model. In Table 3 it is shown that the three kidney "corrected" mean values are within 15% of each other, while the standard deviation in each case is approximately 50%. Coupled with the fact that the irradiation sites represented by this kidney data were located in many different orientations within the specimen (as noted by widely varying Y coordinate in Appendix D), the consistency of the "corrected" mean absorption coefficients suggest that the dosimetric model is substantiated in the case of kidney irradiation sites.

Attention is turned to the muscle absorption coefficient values. It is shown in Table 3 that the abdominal muscle and first back muscle entry "corrected" mean values are fairly close. The second back muscle entry is composed of back muscle irradiation sites which were under the spine. These sites are denoted by asterisks in Appendix D. The "corrected" mean for this entry is an order of magnitude larger than the other back muscle "corrected" mean values. This absorption coefficient discrepancy arises from a dosimetric model inadequacy. To determine the nature of this inadequacy, the back muscle data were treated on the specimen level. In otherwords, relationships between the back muscle irradiation sites were inspected simultaneously to determine how the acoustic field interacted within the specimen.

The high calculated absorption coefficents for the muscle under the spine are the result of a low calculated "*in situ* intensity", as the dT/dt values obtained from these sites are in the same range as the dT/dt values obtained from back muscle sites not under the spine. This low "*in situ* intensity" is a result of faulty modeling of the interposing tissues. Recall from Section 4.2, that all the tissue boundries were modeled as plane interfaces of infinite lateral extent. Modeling the spinal column as a specular reflector results in an impedance discontinuity which allows only 25% of the incident acoustic intensity to be transmitted. In actuality, the diameter of the spine is 4 mm, which is about twice the wavelength. The scattered and diffracted radiation has a distribution which is both complex and critically dependent upon the dimensions and characteristic impedance of the spinal column. Furthermore, the spinal diameter is approximately the same size as the minimum cross-sectional beam diameter (Dt). Thus, the spinal column will not interact with the entire acoustic wave as would an infinite interface. It can be concluded therefore, that the dosimetric model must be changed to produce a more suitable "in situ intensity" at irradiation sites which are under the spine.

Another consideration in the area of the spine is heat diffusion. During irradiation, the spinal column temperature will rise faster than the temperature of the surrounding tissues. This is due to the higher absorption coefficient of bone. Thus, a higher temperature rise will be measured in the tissues surrounding the spine than would be expected because of this added spinal heating source. No assumptions were made in the dosimetric model concerning this diffusion phenomena.

The abdominal muscle data were also inspected on the specimen level. Since the "corrected" mean value is fairly close to the literature value, one might infer that the dosimetric model is adequate for abdominal muscle irradiation sites. Upon closer inspection of the MMA data in Appendix D though, an interesting trend was discovered. It appeared that the magnitude of the calculated absorption coefficient was proportional to the depth of the thermocouple junction within the specimen in the direction of the focal axis, that is , in the X direction. The muscle absorption coefficient though, should be independent of the tissue depth. In order to substantiate this trend, the calculated absorption coefficient was plotted against the thermocouple junction depth within the specimen (Figure 18). A first order least squares linear regression model was used to fit the data points. The resulting regression equation was Y=0.02117+0.01425*X. Although this equation produces a line which supports the trend, further analysis was performed to determine if there was significant regression and no lack of fit (Draper and Smith, 1966). The results of this analysis are shown in the Analysis of Variance Table (Table 4). The two values of greatest interest in this table are R and F . The R value measures the proportion of the total variation about the mean Y explained by the regression. In this case R =0.317. Thus, the regression equation obtained explains only 31.7% of the total variation. The F value denotes the significance of the lack of fit. From Table 4, F=7.0 suggests that the lack of fit is significant. These two values indicate the first order regression equation obtained here is inadequate in describing the data points. A higher order regression model might be used to fit the data points. With the data presently available, the suspicion that the calculated absorption coefficient is proportional to the depth can not be substantiated. Further investigation to

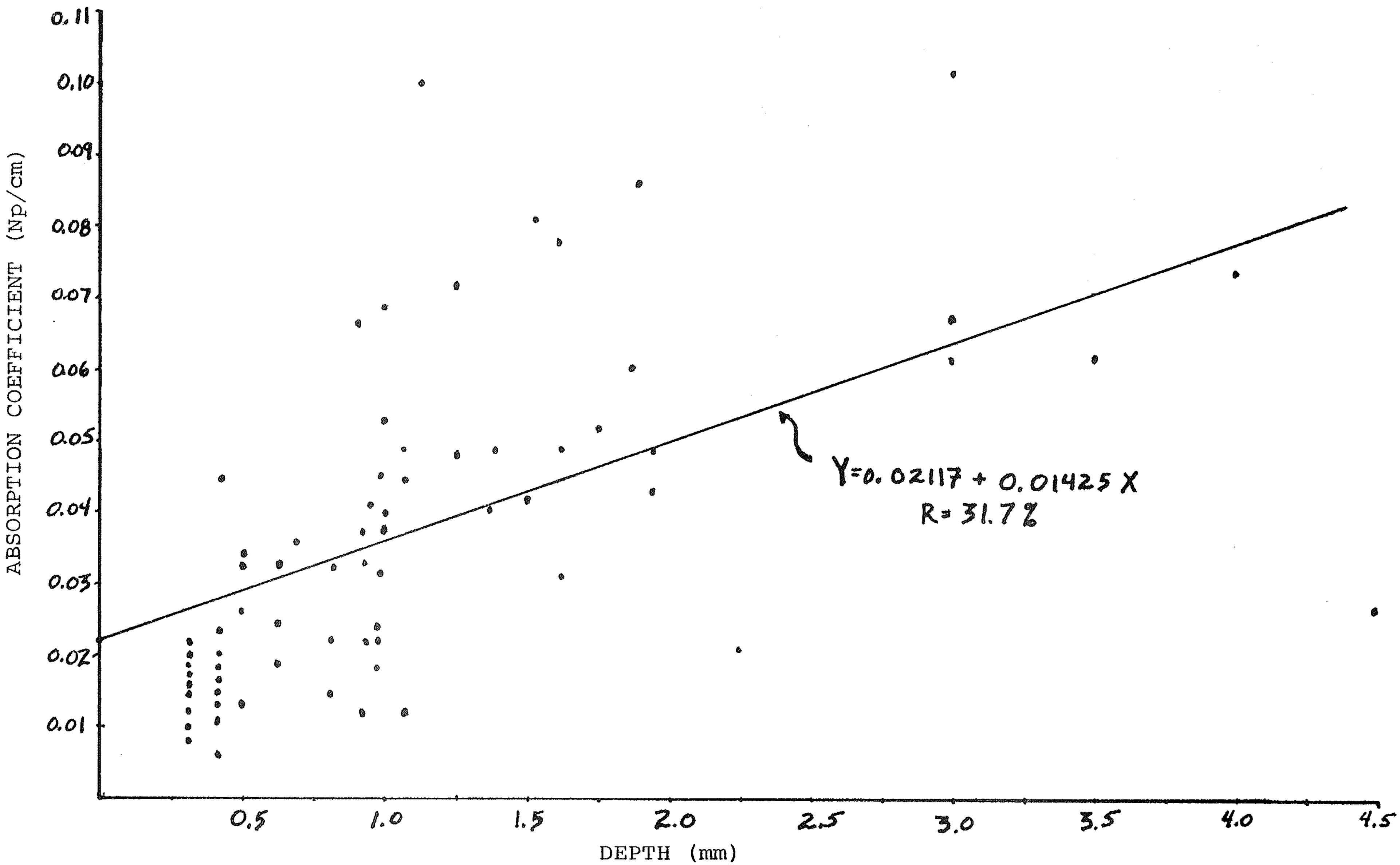

Figure 18. Absorption coefficient vs. tissue depth in direction of focal axis for abdominal muscle tissue

Table 4: Analysis of Variance Table

Source	Degrees of Freeedom	Sum of Squares	Mean Square	
Total	66	0.03624		R =0.317
Regression	1	0.01149	0.01149	F =30.24
Residual	65	0.02474	0.00038	
Lack of Fit	21	0.01901	0.00091	F =7.0
Pure Error	44	0.00573	0.00013	

increase the data base size might produce data points which yield a significant regression equation with no lack of fit.

During the course of obtaining the irradiation data it was suspected that the angle of incidence of the acoustic beam with respect to the specimen affected the thermocouple output. This suspicion arose in a number of specimens in which the thermocouple was inserted just under the skin. As the junction was pulled through the mouse higher dT/dt values were measured at in the central irradiation sites (normal acousic incidence) than at sites near the skin perforations (oblique incidence). In a few specimens though, higher dT/dt values were measured close to skin perforations. Since the irradiation sites near the perforations were the same tissue as those in the center of the mouse (skin/abdominal muscle interface), these dT/dt differences were not expected. Figure 19 is a comparison of specimens 25, 30 and 52. Plotted is the calculated absorption coefficient vs. thermocouple position along the Y axis. These three specimens had thermocouple paths which were virtually identical in terms of the constituent tissues. Figure 19 shows that specimens 30 and 52 are examples of the first case. The central irradiation sites have a supposedly higher absorption coefficient than the identical tissues near the skin perforations. Specimen 25 shows the opposite trend. It can be seen in all three specimens that there is an increase

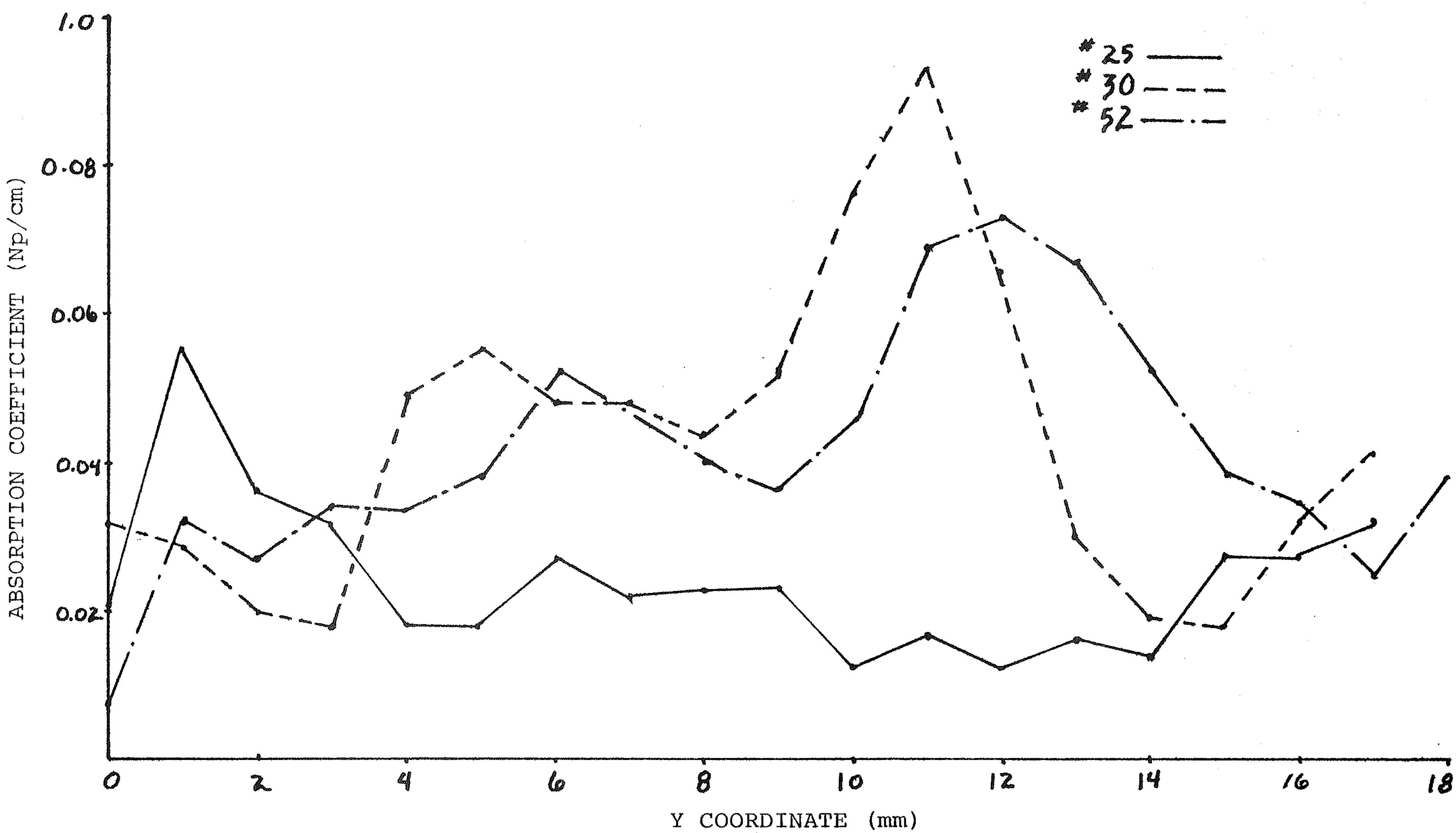

Figure 19. Aborption coefficient vs. thermocouple junction position on Y axis for abdominal muscle tissue in specimens numbered 25, 30, and 52

in the calculated absorption coefficient very close to the skin perforation. This is most likely due to the higher absorption coefficient of skin. It can not be concluded from this data whether or not acoustic incidence affects the determination of the absorption coefficient. This issue must be settled as new experimental procedures and data analysis algorithms would have to be developed if it were shown the assumption of normal acoustic incidence could not be substantiated at each irradiation site.

In summary, it has been shown that using computer files to manipulate the experimental data provides a successful means of achieving complex dosimetric analysis. The results of this analysis have shown the dosimetric model used to calculate the "*in situ* intensity" to be incomplete. Allowances must be made for: 1) tissue boundaries which can not be modeled as infinite planes normal to the focal axis; 2) possible heat diffusion effects; 3) possible refraction of the acoustic beam at tissue boundaries. Combining these factors with the valid assumptions made in the first model, a second generation dosimetric model may be proposed.

CHAPTER 5

CONCLUSION

The results discussed in the previous chapter show the approach used in the experiment to obtain dosimetric information is valid. Although the first generation dosimetric model was shown to have some inadequacies, a number of interesting interactions between the ultrasonic beam and the specimen tissues were characterized. It has been shown that the transient thermoelectric technique was well suited for this application, and the associated irradiation instrumentation used to implement the data acquisition algorithm was adequate. The histological sectioning techniques developed here were not only valuable in this experiment, but may also be applied to other types of specimens. The data analysis performed in this study was primarily completed to substantiate the dosimetric model. Unfortunately, little progress was made in identifying a dosimetric parameter. Before this parameter can be realized, a number of steps must be taken to improve the experimental procedure, instrumentation, and data analysis techniques. The purpose of this chapter is to suggest possible experimental improvements, which upon implementation, will yield a complete dosimetric analysis.

In reviewing the experimental procedure, it becomes clear that the inherent flaw in this experiment is the uncertainty in the calculated "*in situ* intensity". This intensity value was completely dependent upon the accuracy of the dosimetric model. If the interposing tissues were modeled incorrectly or beam refraction effects were present, an erroneous value for the tissue absorption coefficient would be obtained. Thus, an accurate method of obtaining the "*in situ* intensity" is imperative for experimental success. It would be desirable to measure the "*in situ* intensity" directly. The probe used to measure this intensity must produce a response which is independent of the surrounding tissues. Such a probe can be developed using the transient thermoelectric technique. The thermocouple junction is encased in a small bolus of polyethylene or epoxy resin to isolate the junction from the tissue. The absorption coefficients of these embedding materials can be determined. Using a short acoustic pulse (0.1 sec) to assure the heat from the surrounding tissue does not diffuse into the bolus, the thermocouple response used with equation 9 will yield the "*in situ* intensity". To investigate the tissue absorption coefficient at the irradiation site, the encased junction could be combined with a naked junction into a single thermocouple wire. These junctions would be separated by a distance of 3 cm to assure only one junction at a time is affected by the acoustic beam. To obtain both the α and Is at an irradiation site, the encased junction is first pulled into the site and irradiated with a short pulse. From the received thermocouple response the "*in situ* intesity" may be calculated. The naked thermocouple junction is then moved into the irradiation site, and irradiated with a one second pulse. This response, combined with the "*in situ* intensity" found moments earlier, will yield an accurate absorption coefficient value. This double junction probe will be especially useful in tissues which are difficult to model such as the intestinal organs and tissues surrounding the spine.

To successfully implement the procedures involved with this double junction probe, precise control over the positions of the junctions must be obtained. The present specimen structure does not provide this control. Furthermore, this structure is not physically large enough to move both junctions (3 cm apart) through an entire specimen. A new structure which does not have these liabilities has been built (Vaughn, 1980). This structure has a number of advantages over the specimen structure described in Section 3.2. They are: 1) precise computer controlled motor driven thermocouple junction positioning; 2) freedom of mouse orientation with respect to the specimen structure to allow greater thermocouple path choice; 3) multiple thermocouple wires may be used; 4)covered thermocouple lead connectors to allow saline acoustic propagation solutions to be used; 5)coaxial thermocouple leads; 6)fewer Plexiglas obstructions around the specimen. The use of this specimen structure provides a means of changing the orientation of the mouse with respect to the focal axis as well as the ability to probe different tissue combinations.

To fully examine the interactions of the acoustic beam and the tissues within the specimen, *in vivo* beam profiling should be done. Steps have already been taken to mechanize this profiling procedure(Vaughn,1980). The milling base has been placed under computer control. Sychronized movements of the thermocouple probe and milling base can be produced by programming the Interdata minicomputer. The output of a new data acquisition system is also fed to the Interdata. This system consists of a 2 stage amplifier which accepts the thermocouple response and an A/D converter. Thus, all the thermocouple responses can be digitized, analyzed and stored for later use.

In this digitized form the thermocouple responses can be analyzed in a number of ways (Duback, 1980). The time rate of change of temperature can be investigated at any instant of the response. This investigation may yield information concerning heat diffusion effects. Detailed examination of the viscous rise may suggest a method for the characterization of different tissues. It must be noted that the dT/dt value was a parameter not examined in Chapter 4. This value is a direct indication of the energy absorbed by the irradiated tissue. Therefore, the dT/dt values should be closely examined in further dosimetric analysis.

In summary, it has been shown that the approach and experimental procedures discussed in this thesis provide useful information for dosimetric analysis. In the continuation of this study, the changes to the dosimetric model proposed in Chapter 4 should be incorporated into a second generation model. Using this new model, the new instrumentation described above, and the experimental procedures and data compilation techniques described in Chapters 3 and 4, the information necessary to develop a total dosimetric concept will be obtained. Once this concept is complete, ultrasound may be used with greater confidence in medical applications.

REFERENCES

AIUM/NEMA Safety Standard for Diagnostic Ultrasound Equipment. (Draft IV, December 19, 1979).

Bamber, J. C., M. J. Fry, C. R. Hill, and F. Dunn. Ultrasonic Attenuation and Backscattering by Mammalian Organs as a Function of Time After Excision. Ultrasound in Med. Biol. 3:15-20, Pergamon Press, 1979.

Bang, J. The Intensity of Ultrasound in the Uterus During Examination for Diagnostic Purposes. Acta Path. 80:341-344, 1972.

Draper, N. and H. Smith. APPLIED REGRESSION ANALYSIS. John Wiley and Sons, New York, 1966.

Dunn, F. and W. J. Fry. Precision Calibration of Ultrasonic Fields by Thermoelectric Probes. Paper presented at IRE National Convention, NY, 1957.

Dunn, F., A. J. Averbach, and W. D. O'Brien, Jr. A Primary Method for the Determination of Ultrasonic Intensity with the Elastic Sphere Radiometer. Acustica, 38:56-61, 1977

Duback, D. Thesis for the Degree of Master of Science in Electrical Engineering, University of Illinois, 1980, in preparation.

ELECTRONICS, Vol 52, Magraw Hill, NY, Jan. 4, 1979.

Fry, W. J. and R. B. Fry. Determination of Absolute Sound Levels and Acoustic Absorption Coefficients by Thermocouple Probes--Theory. J. Acoust. Soc. Am. 26:294-310, 1954a.

Fry, W. J. and R. B. Fry. Determination of Absolute Sound Levels and Acoustic Absorption Coefficients by Thermocouple Probes--Experiment. J. Acoust. Soc. Am. 26:311-317, 1954b.

Fry, W. J. and F. Dunn. Ultrasound: Analysis and Experimental Methods in Biological Research. In PHY. TECH. BIOL. RES. 4:261-394, 1962.

Goss, S. A. J. W. Cobb, and L. A. Frizzell. Effect of Beam Width and Thermocouple Size on the Measurement of Ultrasonic Absorption Using the Thermoelectric Technique. In 1977 Ultrasonics Symposium, ed. J. de Klerk and B. R. McAvoy, pp. 206-211, IEEE Catalog No. 77CH1264-ISU, New York, 1977.

Goss, S. A., R. L. Johnston, and F. Dunn. Comprehensive Compilation of Empirical Ultrasonic Properties of Mammalian Tissues. J. Acoust. Soc. Am. 64:423-457, 1978

Goss, S. A., L. A. Frizzell, and F. Dunn. Ultrasonic Absorption and Attenuation in Mammalian Tissues. Ultrasound Med. Biol 5:,181-186, 1979.

Hall, A. J. and H. P. Robinson. Transmitted Ultrasonic Energy Levels in the Nongravid Uterus. Colloquim on Ultrasound Bioeffects and Dosimetry, London, July 22-23, 1974, (abstract).

Hueter T. F. and R. N. Bolt. SONICS. John Wiley and Sons, New York, 1955.

Johnston, R. L. and F. Dunn. Ultrasonic Absorbed Dose, Dose Rate, and Produced Lesion Volume. Ultrasonics 14:153-155, 1976.

Kinsler, L. and A. Frey. FUNDAMENTALS OF ACOUSTICS. John Wiley and Sons, New York, 1962.

O'Neil, H. T. Theory of Focusing Radiaters, J. Acoust. Soc. Am. 21:561-574, 1949.

Vaughn, S. T. Thesis for the Degree of Master of Science in Electrical Engineering, University of Illinois, 1980, in preparation.

Wyneken, J. and W. D. O'Brien, Jr. A Method For Analyzing the Path of a Thermocouple Through a Laboratory Mouse. In preparation.

APPENDIX A

EXAMPLE ENTRY FROM IRRADIATION FILE DOSEXPC.DTA

DESCRIPTION OF COLUMNS IS FOUND IN SECTION 4.2

MOUSE#	TC#	Y	X	Z	SHOT#	TC POSITION	DTDT	DEFLECTION	INCIDENT INTENSITY
36	1	0.0	0.0	0.0	1	75	0.73	1.51	38.2
0	0	1.0	0.0	0.0	2	76	0.79	1.56	38.2
0	0	2.0	0.0	0.0	3	77	1.22	2.25	38.2
0	0	3.0	0.0	0.0	4	78	0.97	1.97	38.2
0	0	4.0	0.0	0.0	5	79	0.53	1.04	38.2
0	0	5.0	0.0	0.0	6	80	0.53	0.97	38.2
0	0	6.0	0.0	0.0	7	81	0.46	0.56	38.2
0	0	7.0	0.0	0.0	8	82	0.66	0.73	38.2
0	0	8.0	0.0	0.0	9	83	0.61	0.90	38.2
0	0	9.0	0.0	0.0	10	84	0.47	0.65	38.2
0	0	10.0	0.0	0.0	11	85	0.53	0.62	38.2
0	0	11.0	0.0	0.0	12	86	0.64	1.10	38.2
0	0	12.0	0.0	0.0	13	87	0.46	0.68	38.2
0	0	13.0	0.0	0.0	14	88	0.38	0.47	38.2
0	0	14.0	0.0	0.0	15	89	0.45	0.68	38.2
0	0	15.0	0.0	0.0	16	90	0.96	1.46	38.2
0	0	16.0	0.0	0.0	17	91	0.79	1.37	38.2
0	0	17.0	0.0	0.0	18	92	1.57	2.52	38.2
0	0	18.0	0.0	0.0	19	93	1.60	1.98	38.2
0	0	19.0	0.0	0.0	20	94	1.06	1.37	38.2
0	0	20.0	0.0	0.0	21	95	0.56	0.95	38.2
0	0	21.0	0.0	0.0	22	96	1.36	1.86	38.2
0	0	22.0	0.0	0.0	23	97	1.59	2.90	38.2
0	0	23.0	0.0	0.0	24	98	0.46	0.66	38.2

APPENDIX B

EXAMPLE ENTRY FROM HISTOLOGY FILE DOSHIS.DTA

DESCRIPTION OF COLUMNS IS FOUND IN SECTION 4.3

MOUSE#	TC#	Y	X	Z	DEPTH	TISSUE CODE	INTERPOSING TISSUE							
36	1	0.0	0.0	0.0	0.0	WJD		0.0		0.0		0.0		0.0
0	0	1.0	0.0	0.0	0.2	DER	DER	0.2		0.0		0.0		0.0
0	0	2.0	0.0	0.0	2.0	BLO	DER	0.7	ADP	1.0	BLO	0.3		0.0
0	0	3.0	0.0	0.0	3.3	MJW	DER	0.5	ADP	0.2	MMA	2.6		0.0
0	0	4.0	0.0	0.0	4.5	KIC	DER	0.5	MMA	0.2	KIC	3.8		0.0
0	0	5.0	0.0	0.0	5.2	KIC	DER	0.5	MMA	0.1	KIG	4.6		0.0
0	0	6.0	0.0	0.0	6.2	KIG	DER	0.5	MMA	0.3	KIG	5.4		0.0
0	0	7.0	0.0	0.0	7.0	KIM	DER	0.4	MMA	0.2	ADP	0.1	KIG	6.3
0	0	8.0	0.0	0.0	7.8	KIC	DER	0.4	MMB	1.5	KIG	5.9		0.0
0	0	9.0	0.0	0.0	8.1	KIC	DER	0.3	MMB	2.0	KIG	4.4	BLO	0.3
999	0	9.0	0.0	0.0	8.1	KIC	KIC	1.1		0.0		0.0		0.0
0	0	10.0	0.0	0.0	8.0	BLO	DER	0.4	MMB	3.4	KIG	3.7	BLO	0.5
0	0	11.0	0.0	0.0	7.2	BLO	DER	0.2	MMB	6.2	CNT	0.1	BLO	0.5
0	0	12.0	0.0	0.0	7.0	CNT	DER	0.3	MMB	2.0	NSP	1.0	MMB	3.1
999	0	12.0	0.0	0.0	7.0	CNT	CNT	0.6		0.0		0.0		0.0
0	0	13.0	0.0	0.0	7.0	FAS	DER	0.3	MMB	1.4	NSP	2.8	MMB	1.6
999	0	13.0	0.0	0.0	7.0	FAS	FAS	0.9		0.0		0.0		0.0
0	0	14.0	0.0	0.0	6.9	FAS	DER	0.2	MMB	2.0	NSP	1.0	MMB	2.2
999	0	14.0	0.0	0.0	6.9	FAS	ADP	0.9	FAS	0.6		0.0		0.0
0	0	15.0	0.0	0.0	6.8	FAS	DER	0.3	MMB	4.6	ADP	0.2	BLO	1.2
999	0	15.0	0.0	0.0	6.8	FAS	FAS	0.5		0.0		0.0		0.0
0	0	16.0	0.0	0.0	6.5	FAS	DER	0.5	MMB	3.8	ADP	0.5	FAS	1.7
0	0	17.0	0.0	0.0	6.0	FAS	DER	0.5	MMB	2.5	ADP	1.0	FAS	2.0
0	0	18.0	0.0	0.0	5.0	PLG	DER	0.5	MMA	1.1	ADP	1.3	FAS	0.2
999	0	18.0	0.0	0.0	5.0	PLG	PLG	1.4		0.0		0.0		0.0
0	0	19.0	0.0	0.0	3.8	PLG	DER	0.5	MMA	2.1	ADP	0.1	PLG	1.1
0	0	20.0	0.0	0.0	1.7	MMA	DER	0.6	MMA	1.1		0.0		0.0
0	0	21.0	0.0	0.0	1.2	MMA	DER	0.4	MMA	0.8		0.0		0.0
0	0	22.0	0.0	0.0	0.2	DER	DER	0.2		0.0		0.0		0.0
0	0	23.0	0.0	0.0	0.0	DJW		0.0		0.0		0.0		0.0

APPENDIX C

EXAMPLE ENTRY FROM DOSIMETRIC FILE DOS.DTA

DESCRIPTION OF COLUMNS IS FOUND IN SECTION 4.4

MOUSE#	TC#	Y	X	Z	TISSUE CODE	DEPTH(MM)	DTDT(DEG/SEC)	I(W/CM2)	ALPHA(NP/CM)
36	1	0.0	0.0	0.0	WJD	0.0	0.73	38.2	0.036
36	0	1.0	0.0	0.0	DER	0.2	0.79	37.3	0.040
36	0	2.0	0.0	0.0	BLO	2.0	1.22	34.9	0.066
36	0	3.0	0.0	0.0	MJW	3.3	0.97	32.9	0.056
36	0	4.0	0.0	0.0	KIC	4.5	0.53	33.4	0.030
36	0	5.0	0.0	0.0	KIC	5.2	0.53	32.9	0.030
36	0	6.0	0.0	0.0	KIG	6.2	0.46	32.1	0.027
36	0	7.0	0.0	0.0	KIM	7.0	0.66	31.2	0.040
36	0	8.0	0.0	0.0	KIC	7.8	0.61	30.7	0.038
36	0	9.0	0.0	0.0	KIC	8.1	0.47	26.1	0.034
36	0	10.0	0.0	0.0	BLO	8.0	0.53	30.5	0.033
36	0	11.0	0.0	0.0	BLO	7.2	0.64	30.5	0.040
36	0	12.0	0.0	0.0	CNT	7.0	0.46	1.6	0.552
36	0	13.0	0.0	0.0	FAS	7.0	0.38	0.6	1.272
36	0	14.0	0.0	0.0	FAS	6.9	0.45	1.7	0.507
36	0	15.0	0.0	0.0	FAS	6.8	0.96	26.3	0.069
36	0	16.0	0.0	0.0	FAS	6.5	0.79	30.2	0.049
36	0	17.0	0.0	0.0	FAS	6.0	1.57	30.8	0.096
36	0	18.0	0.0	0.0	PLG	5.0	1.60	30.7	0.098
36	0	19.0	0.0	0.0	PLG	3.8	1.06	33.1	0.060
36	0	20.0	0.0	0.0	MMA	1.7	0.56	35.3	0.030
36	0	21.0	0.0	0.0	MMA	1.2	1.36	35.9	0.072
36	0	22.0	0.0	0.0	DER	0.2	1.59	37.3	0.080
36	0	23.0	0.0	0.0	DJW	0.0	0.46	38.2	0.023

APPENDIX D

THIS TABLE IS A LISTING OF DOS.DTA DIVIDED BY TISSUE TYPE

COLUMN 1- SPECIMEN NUMBER

COLUMN 2- THERMOCOUPLE NUMBER

COLUMN 3-THERMOCOUPLE JUNCTION COORDINATES WITH RESPECT TO THE SPECIMEN (mm).

COLUMN 4- TISSUE CODE

COLUMN 5- THERMOCOUPLE DEPTH BELOW THE SKIN SURFACE IN THE DIRECTION OF THE FOCAL AXIS (mm)

COLUMN 6- TIME RATE OF CHANGE OF TEMPERATURE (C/SEC)

COLUMN 7- "IN SITU INTENSITY" (W/CM**2)

COLUMN 8- TISSUE ABSORPTION COEFFICIENT (NP/CM)

7	18	0	7.0	0.0	0.0	ADP	0.3	0.80	49.7	0.030
8	18	0	9.0	0.0	0.0	ADP	0.3	0.74	49.7	0.028
10	18	0	13.0	0.0	0.0	ADP	0.3	0.78	49.7	0.030
29	21	0	8.0	0.0	0.0	ADP	3.0	0.32	45.8	0.013
30	22	1	7.0	0.0	0.0	ADP	1.4	0.93	49.3	0.036
31	22	0	9.0	0.0	0.0	ADP	3.1	1.15	48.9	0.044
98	28	0	14.0	0.0	0.0	ADP	1.0	0.37	36.3	0.019
252	38	0	3.0	0.0	0.0	ADP	1.6	0.73	18.7	0.074
253	38	0	4.0	0.0	0.0	ADP	2.4	0.45	18.5	0.046
263	38	0	15.0	0.0	0.0	ADP	4.0	1.08	45.1	0.045
290	39	0	23.0	0.0	0.0	ADP	2.3	1.38	48.1	0.054
315	40	0	23.0	0.0	0.0	ADP	1.2	0.78	49.4	0.030
316	40	0	24.0	0.0	0.0	ADP	1.0	0.95	49.6	0.036
320	41	0	1.0	0.0	0.0	ADP	0.8	1.05	18.8	0.106
364	42	0	22.0	0.0	0.0	ADP	1.1	0.31	11.8	0.049
366	43	0	1.0	0.0	0.0	ADP	1.7	0.81	11.7	0.131
390	44	0	1.0	0.0	0.0	ADP	1.1	0.42	35.9	0.022
404	44	0	15.0	0.0	0.0	ADP	7.7	0.35	1.6	0.402
416	47	0	1.0	0.0	0.0	ADP	2.3	0.81	17.7	0.087
417	47	0	2.0	0.0	0.0	ADP	3.1	0.60	17.9	0.063
461	51	0	1.0	0.0	0.0	ADP	3.0	0.72	17.1	0.079
462	51	0	2.0	0.0	0.0	ADP	3.6	0.83	34.6	0.045
482	51	0	22.0	0.0	0.0	ADP	1.7	0.17	18.0	0.018
495	52	0	12.0	0.0	0.0	ADP	1.0	1.01	26.2	0.073
496	52	0	13.0	0.0	0.0	ADP	0.8	0.94	26.6	0.067
497	52	0	14.0	0.0	0.0	ADP	0.7	0.74	26.7	0.052
501	52	0	18.0	0.0	0.0	ADP	0.5	0.52	26.7	0.037
503	53	0	2.0	0.0	0.0	ADP	0.6	0.00	18.8	0.000
504	53	0	4.0	0.0	0.0	ADP	0.7	1.34	18.7	0.136
505	53	0	6.0	0.0	0.0	ADP	0.8	0.56	18.6	0.057
506	53	0	8.0	0.0	0.0	ADP	0.8	0.46	18.6	0.047
507	53	0	10.0	0.0	0.0	ADP	0.7	0.39	18.7	0.040
508	53	0	12.0	0.0	0.0	ADP	0.9	0.39	18.5	0.040
509	53	0	13.0	0.0	0.0	ADP	0.8	0.26	12.1	0.040
12	19	1	1.0	0.0	0.0	DJA	0.3	0.53	50.7	0.020
13	19	0	3.0	0.0	0.0	DJA	0.2	0.54	50.9	0.020
254	38	0	5.0	0.0	0.0	AJM	3.0	0.39	17.7	0.042
363	42	0	21.0	0.0	0.0	MJA	2.2	0.56	11.5	0.092

168	33	0	12.0	0.0	0.0	BLO	9.7	0.22	24.6	0.017
189	34	0	9.0	0.0	0.0	BLO	7.5	0.41	30.7	0.025
205	36	0	2.0	0.0	0.0	BLO	2.0	1.22	34.9	0.066
213	36	0	10.0	0.0	0.0	BLO	8.0	0.53	30.5	0.033
214	36	0	11.0	0.0	0.0	BLO	7.2	0.64	30.5	0.040
277	39	0	9.0	0.0	0.0	BLO	8.0	1.06	40.5	0.049
376	43	0	11.0	0.0	0.0	BLO	8.8	0.56	1.9	0.563
378	43	0	13.0	0.0	0.0	BLO	8.8	0.74	21.1	0.066
379	43	0	14.0	0.0	0.0	BLO	8.2	0.91	28.9	0.059
399	44	0	10.0	0.0	0.0	BLO	8.6	0.64	28.7	0.042

400	44	0	11.0	0.0	0.0	BLO	8.5	0.30	21.9	0.026
401	44	0	12.0	0.0	0.0	BLO	8.3	0.20	29.3	0.013
303	40	0	11.0	0.0	0.0	BVV	7.3	0.40	2.1	0.357
377	43	0	12.0	0.0	0.0	BVV	9.0	0.24	3.3	0.137
402	44	0	13.0	0.0	0.0	BVV	8.2	0.21	0.4	0.921
403	44	0	14.0	0.0	0.0	BVV	7.9	0.31	0.4	1.360
427	47	0	12.0	0.0	0.0	BVV	6.3	0.27	0.3	1.620
472	51	0	12.0	0.0	0.0	BVV	5.3	0.44	5.2	0.161
235	37	0	9.0	0.0	0.0	BJV	7.0	0.46	19.4	0.045
236	37	0	10.0	0.0	0.0	BJV	7.3	0.27	23.3	0.022
191	34	0	11.0	0.0	0.0	MJB	8.2	1.20	7.5	0.301
193	34	0	13.0	0.0	0.0	MJB	8.1	0.52	29.3	0.034
2	17	0	2.0	0.0	0.0	CNT	1.5	0.96	48.3	0.038
3	17	0	4.0	0.0	0.0	CNT	1.2	0.92	48.8	0.036
5	17	0	8.0	0.0	0.0	CNT	0.6	1.37	50.1	0.052
169	33	0	13.0	0.0	0.0	CNT	9.8	0.17	25.2	0.013
170	33	0	14.0	0.0	0.0	CNT	9.7	0.18	20.8	0.016
215	36	0	12.0	0.0	0.0	CNT	7.0	0.46	1.6	0.552
237	37	0	11.0	0.0	0.0	CNT	7.8	0.23	18.4	0.024
238	37	0	12.0	0.0	0.0	CNT	8.0	0.21	19.3	0.021
278	39	0	10.0	0.0	0.0	CNT	9.2	0.67	1.5	0.862
354	42	0	12.0	0.0	0.0	CNT	7.6	1.83	1.5	2.349
426	47	0	11.0	0.0	0.0	CNT	6.1	0.85	5.9	0.270
355	42	0	13.0	0.0	0.0	CJM	7.8	2.45	5.5	0.839
37	23	0	5.0	0.0	0.0	CRU	3.7	0.94	45.4	0.039
38	23	0	7.0	0.0	0.0	CRU	4.1	3.25	11.5	0.535
39	23	0	8.0	0.0	0.0	CRU	4.1	1.44	44.2	0.062
44	24	1	9.0	0.0	0.0	CRU	1.5	1.52	46.7	0.061
45	24	0	10.0	0.0	0.0	CRU	1.4	1.74	47.1	0.070
46	24	0	11.0	0.0	0.0	CRU	1.4	2.73	46.2	0.112
89	28	0	5.0	0.0	0.0	CRU	0.6	0.69	36.1	0.036
92	28	0	8.0	0.0	0.0	CRU	0.7	0.54	35.8	0.028
93	28	0	9.0	0.0	0.0	CRU	0.8	0.42	18.4	0.043
94	28	0	10.0	0.0	0.0	CRU	0.9	0.44	18.3	0.046
172	33	0	16.0	0.0	0.0	CRU	9.0	0.17	26.9	0.012
173	33	0	17.0	0.0	0.0	CRU	8.8	0.00	15.2	0.000
174	33	0	18.0	0.0	0.0	CRU	8.5	0.12	15.7	0.014
175	33	0	19.0	0.0	0.0	CRU	8.0	0.21	16.3	0.024
176	33	0	20.0	0.0	0.0	CRU	7.5	0.19	17.0	0.021
25	20	0	13.0	0.0	0.0	DER	0.2	0.34	50.9	0.013
51	24	0	17.0	0.0	0.0	DER	0.1	0.32	51.2	0.012
54	25	0	1.0	0.0	0.0	DER	0.5	1.45	50.2	0.055

69	25	0	16.0	0.0	0.0	DER	0.5	0.69	50.2	0.026
85	28	0	1.0	0.0	0.0	DER	0.1	0.49	37.5	0.025
86	28	0	2.0	0.0	0.0	DER	0.2	0.42	37.3	0.021
115	29	0	16.0	0.0	0.0	DER	0.2	0.72	50.9	0.027
151	32	0	1.0	0.0	0.0	DER	0.2	0.08	19.3	0.008
157	33	0	1.0	0.0	0.0	DER	1.8	0.82	27.3	0.057
204	36	0	1.0	0.0	0.0	DER	0.2	0.79	37.3	0.040
225	36	0	22.0	0.0	0.0	DER	0.2	1.59	37.3	0.080
250	38	0	1.0	0.0	0.0	DER	0.2	0.80	19.3	0.078
267	38	0	21.0	0.0	0.0	DER	0.2	1.32	2.7	0.912
269	39	0	1.0	0.0	0.0	DER	0.2	0.53	50.9	0.020
293	40	0	1.0	0.0	0.0	DER	1.8	0.59	19.4	0.058
340	41	0	21.0	0.0	0.0	DER	0.2	1.34	19.3	0.131
388	43	0	23.0	0.0	0.0	DER	0.6	1.17	36.6	0.060
389	44	1	0.0	0.0	0.0	DER	0.0	0.12	38.2	0.006
414	44	0	25.0	0.0	0.0	DER	0.0	0.26	7.4	0.066
415	47	1	0.0	0.0	0.0	DER	0.0	1.52	19.8	0.145
436	50	0	1.0	0.0	0.0	DER	2.4	0.52	34.0	0.029
12	19	1	1.0	0.0	0.0	DJA	0.3	0.53	50.7	0.020
13	19	0	3.0	0.0	0.0	DJA	0.2	0.54	50.9	0.020
19	20	1	1.0	0.0	0.0	DJM	0.2	0.39	50.9	0.014
20	20	0	3.0	0.0	0.0	DJM	0.2	0.49	50.9	0.018
21	20	0	5.0	0.0	0.0	DJM	0.3	0.59	50.7	0.022
22	20	0	7.0	0.0	0.0	DJM	0.5	0.58	49.8	0.022
24	20	0	11.0	0.0	0.0	DJM	0.2	0.45	50.9	0.017
55	25	0	2.0	0.0	0.0	DJM	0.3	0.96	50.5	0.036
56	25	0	3.0	0.0	0.0	DJM	0.2	0.86	50.9	0.032
57	25	0	4.0	0.0	0.0	DJM	0.3	0.50	50.7	0.019
58	25	0	5.0	0.0	0.0	DJM	0.3	0.47	50.7	0.018
59	25	0	6.0	0.0	0.0	DJM	0.3	0.72	50.7	0.027
60	25	0	7.0	0.0	0.0	DJM	0.2	0.59	50.9	0.022
61	25	0	8.0	0.0	0.0	DJM	0.3	0.62	50.7	0.023
62	25	0	9.0	0.0	0.0	DJM	0.3	0.63	50.7	0.023
63	25	0	10.0	0.0	0.0	DJM	0.4	0.34	50.3	0.013
64	25	0	11.0	0.0	0.0	DJM	0.3	0.46	50.7	0.017
65	25	0	12.0	0.0	0.0	DJM	0.2	0.33	50.9	0.012
66	25	0	13.0	0.0	0.0	DJM	0.4	0.42	50.4	0.016
67	25	0	14.0	0.0	0.0	DJM	0.5	0.38	50.2	0.014
68	25	0	15.0	0.0	0.0	DJM	0.6	0.68	48.5	0.027
99	28	0	15.0	0.0	0.0	DJM	0.6	0.30	36.7	0.015
114	29	0	15.0	0.0	0.0	DJM	0.6	0.32	50.0	0.012
118	30	0	1.0	0.0	0.0	DJM	0.8	0.76	49.5	0.029
119	30	0	2.0	0.0	0.0	DJM	0.7	0.53	49.7	0.020
120	30	0	3.0	0.0	0.0	DJM	0.6	0.48	49.9	0.018
121	30	0	4.0	0.0	0.0	DJM	0.6	1.30	49.9	0.049
122	30	0	5.0	0.0	0.0	DJM	0.5	1.46	50.2	0.055
123	30	0	6.0	0.0	0.0	DJM	0.5	1.28	50.2	0.048
124	30	0	7.0	0.0	0.0	DJM	0.6	1.27	49.9	0.048
125	30	0	8.0	0.0	0.0	DJM	0.7	1.16	49.7	0.044
126	30	0	9.0	0.0	0.0	DJM	0.6	1.37	49.9	0.052
127	30	0	10.0	0.0	0.0	DJM	0.6	2.02	49.9	0.076

128	30	0	11.0	0.0	0.0	DJM	0.7	2.44	49.7	0.093
131	30	0	14.0	0.0	0.0	DJM	0.7	0.50	49.7	0.019
132	30	0	15.0	0.0	0.0	DJM	0.6	0.47	50.0	0.018
133	30	0	16.0	0.0	0.0	DJM	0.4	0.85	50.4	0.032
135	31	1	1.0	0.0	0.0	DJM	0.2	0.43	50.9	0.016
148	31	0	15.0	0.0	0.0	DJM	0.6	0.45	50.0	0.017
227	37	1	1.0	0.0	0.0	DJM	1.2	0.91	26.3	0.065
103	28	0	19.0	0.0	0.0	MJD	0.2	0.46	37.3	0.023
149	31	0	16.0	0.0	0.0	MJD	0.1	0.37	51.2	0.014
317	40	0	25.0	0.0	0.0	MJD	0.3	0.95	50.7	0.035
11	18	0	15.0	0.0	0.0	DJW	0.0	0.38	52.1	0.014
52	24	0	18.0	0.0	0.0	DJW	0.0	0.72	52.1	0.026
70	25	0	17.0	0.0	0.0	DJW	0.0	0.88	52.1	0.032
104	28	0	20.0	0.0	0.0	DJW	0.0	0.22	38.2	0.011
116	29	0	17.0	0.0	0.0	DJW	0.0	0.18	52.1	0.007
134	30	0	17.0	0.0	0.0	DJW	0.0	1.12	52.1	0.041
179	33	0	23.0	0.0	0.0	DJW	0.0	0.39	30.2	0.024
202	34	0	22.0	0.0	0.0	DJW	0.0	0.69	38.2	0.034
226	36	0	23.0	0.0	0.0	DJW	0.0	0.46	38.2	0.023
248	37	0	22.0	0.0	0.0	DJW	0.0	0.25	28.3	0.017
318	40	0	26.0	0.0	0.0	DJW	0.0	0.70	52.1	0.025
341	41	0	22.0	0.0	0.0	DJW	0.0	1.11	19.8	0.106
459	50	0	24.0	0.0	0.0	DJW	0.0	0.45	38.2	0.022
460	51	1	0.0	0.0	0.0	DJW	0.0	0.69	19.8	0.066
483	52	1	0.0	0.0	0.0	DJW	0.0	0.14	28.3	0.009
502	53	1	0.0	0.0	0.0	DJW	0.0	0.35	19.8	0.033
1	17	1	0.0	0.0	0.0	WJD	0.0	0.08	52.1	0.003
53	25	1	0.0	0.0	0.0	WJD	0.0	0.58	52.1	0.021
71	26	1	0.0	0.0	0.0	WJD	0.0	0.72	52.1	0.026
84	28	1	0.0	0.0	0.0	WJD	0.0	0.75	38.2	0.037
117	30	1	0.0	0.0	0.0	WJD	0.0	0.85	52.1	0.031
150	32	1	0.0	0.0	0.0	WJD	0.0	0.08	19.8	0.008
156	33	1	0.0	0.0	0.0	WJD	0.0	0.71	30.2	0.044
180	34	1	0.0	0.0	0.0	WJD	0.0	1.29	38.2	0.064
203	36	1	0.0	0.0	0.0	WJD	0.0	0.73	38.2	0.036
249	38	1	0.0	0.0	0.0	WJD	0.0	1.11	19.8	0.106
268	39	1	0.0	0.0	0.0	WJD	0.0	0.39	52.1	0.014
292	40	1	0.0	0.0	0.0	WJD	0.0	0.47	21.4	0.042
319	41	1	0.0	0.0	0.0	WJD	0.0	1.14	19.8	0.109
342	42	1	0.0	0.0	0.0	WJD	0.0	0.84	38.2	0.042
365	43	1	0.0	0.0	0.0	WJD	0.0	0.73	12.9	0.107
435	50	1	0.0	0.0	0.0	WJD	0.0	0.20	38.2	0.010

216	36	0	13.0	0.0	0.0	FAS	7.0	0.38	0.6	1.272
217	36	0	14.0	0.0	0.0	FAS	6.9	0.45	1.7	0.507
218	36	0	15.0	0.0	0.0	FAS	6.8	0.96	26.3	0.069
219	36	0	16.0	0.0	0.0	FAS	6.5	0.79	30.2	0.049
220	36	0	17.0	0.0	0.0	FAS	6.0	1.57	30.8	0.096
229	37	0	3.0	0.0	0.0	FAS	4.3	0.98	21.6	0.086

305	40	0	13.0	0.0	0.0	FAS	6.7	0.46	40.8	0.021
450	50	0	15.0	0.0	0.0	FAS	6.4	0.45	30.1	0.028
451	50	0	16.0	0.0	0.0	FAS	6.1	0.84	30.3	0.052
35	23	1	1.0	0.0	0.0	MJF	1.3	0.56	49.0	0.022
72	26	0	1.0	0.0	0.0	MJF	1.0	0.76	50.0	0.029
304	40	0	12.0	0.0	0.0	MJF	6.8	0.39	2.6	0.284
279	39	0	11.0	0.0	0.0	GUG	8.4	1.88	10.2	0.349
280	39	0	12.0	0.0	0.0	GUG	8.2	0.12	39.6	0.006
182	34	0	2.0	0.0	0.0	KIC	4.5	0.63	32.7	0.036
207	36	0	4.0	0.0	0.0	KIC	4.5	0.53	33.4	0.030
208	36	0	5.0	0.0	0.0	KIC	5.2	0.53	32.9	0.030
211	36	0	8.0	0.0	0.0	KIC	7.8	0.61	30.7	0.038
212	36	0	9.0	0.0	0.0	KIC	8.1	0.47	26.1	0.034
239	37	0	13.0	0.0	0.0	KIC	8.1	0.20	1.1	0.352
240	37	0	14.0	0.0	0.0	KIC	7.8	0.34	2.0	0.317
243	37	0	17.0	0.0	0.0	KIC	5.7	0.46	24.0	0.036
244	37	0	18.0	0.0	0.0	KIC	5.0	0.57	23.5	0.046
272	39	0	4.0	0.0	0.0	KIC	5.2	2.14	43.6	0.093
275	39	0	7.0	0.0	0.0	KIC	7.3	0.82	37.2	0.042
282	39	0	14.0	0.0	0.0	KIC	7.6	0.31	41.1	0.014
295	40	0	3.0	0.0	0.0	KIC	3.8	0.26	45.5	0.011
296	40	0	4.0	0.0	0.0	KIC	4.0	0.15	44.9	0.006
299	40	0	7.0	0.0	0.0	KIC	7.1	0.55	33.3	0.031
300	40	0	8.0	0.0	0.0	KIC	7.4	0.39	40.0	0.018
306	40	0	14.0	0.0	0.0	KIC	6.3	0.73	33.5	0.041
307	40	0	15.0	0.0	0.0	KIC	6.2	0.47	34.7	0.026
311	40	0	19.0	0.0	0.0	KIC	5.8	0.00	50.1	0.000
321	41	0	2.0	0.0	0.0	KIC	2.0	0.67	18.4	0.069
325	41	0	6.0	0.0	0.0	KIC	4.7	0.44	32.6	0.025
333	41	0	14.0	0.0	0.0	KIC	5.0	0.45	6.2	0.136
334	41	0	15.0	0.0	0.0	KIC	5.0	0.39	6.3	0.117
337	41	0	18.0	0.0	0.0	KIC	3.0	1.12	33.0	0.064
338	41	0	19.0	0.0	0.0	KIC	2.1	1.39	35.7	0.074
344	42	0	2.0	0.0	0.0	KIC	2.8	0.71	33.8	0.040
345	42	0	3.0	0.0	0.0	KIC	4.0	0.72	33.1	0.041
353	42	0	11.0	0.0	0.0	KIC	7.5	0.78	29.8	0.050
369	43	0	4.0	0.0	0.0	KIC	4.0	0.41	10.2	0.076
370	43	0	5.0	0.0	0.0	KIC	6.0	0.46	9.8	0.089
371	43	0	6.0	0.0	0.0	KIC	6.5	0.40	24.2	0.031
372	43	0	7.0	0.0	0.0	KIC	7.5	0.10	23.9	0.008
373	43	0	8.0	0.0	0.0	KIC	8.5	0.00	21.5	0.000
375	43	0	10.0	0.0	0.0	KIC	9.2	0.50	4.3	0.219
391	44	0	2.0	0.0	0.0	KIC	2.8	0.91	34.4	0.050
406	44	0	17.0	0.0	0.0	KIC	17.0	0.51	30.1	0.032
407	44	0	18.0	0.0	0.0	KIC	6.1	0.71	31.0	0.043

408	44	0	19.0	0.0	0.0	KIC	5.5	1.04	27.4	0.072
418	47	0	3.0	0.0	0.0	KIC	4.4	0.62	17.1	0.069
423	47	0	8.0	0.0	0.0	KIC	6.3	4.72	16.2	0.551
431	47	0	16.0	0.0	0.0	KIC	16.0	0.50	16.5	0.057
441	50	0	6.0	0.0	0.0	KIC	7.1	0.39	25.6	0.029
442	50	0	7.0	0.0	0.0	KIC	7.3	0.40	29.5	0.026
443	50	0	8.0	0.0	0.0	KIC	7.6	0.58	29.3	0.037
444	50	0	9.0	0.0	0.0	KIC	8.0	0.54	29.0	0.035
445	50	0	10.0	0.0	0.0	KIC	8.1	0.40	28.8	0.026
446	50	0	11.0	0.0	0.0	KIC	8.3	0.62	29.1	0.040
453	50	0	18.0	0.0	0.0	KIC	5.7	0.46	30.9	0.028
463	51	0	3.0	0.0	0.0	KIC	4.2	0.84	34.7	0.046
464	51	0	4.0	0.0	0.0	KIC	4.8	0.92	31.9	0.054
469	51	0	9.0	0.0	0.0	KIC	5.2	0.15	32.1	0.009
475	51	0	15.0	0.0	0.0	KIC	5.8	0.63	31.6	0.038
479	51	0	19.0	0.0	0.0	KIC	5.0	1.40	29.7	0.089
183	34	0	3.0	0.0	0.0	KIM	5.0	0.46	32.4	0.027
184	34	0	4.0	0.0	0.0	KIM	5.5	0.60	32.0	0.035
185	34	0	5.0	0.0	0.0	KIM	5.8	0.61	31.8	0.036
186	34	0	6.0	0.0	0.0	KIM	5.6	0.46	32.0	0.027
210	36	0	7.0	0.0	0.0	KIM	7.0	0.66	31.2	0.040
241	37	0	15.0	0.0	0.0	KIM	7.5	0.34	22.5	0.029
242	37	0	16.0	0.0	0.0	KIM	6.8	0.34	23.2	0.028
273	39	0	5.0	0.0	0.0	KIM	6.0	1.67	42.2	0.075
274	39	0	6.0	0.0	0.0	KIM	7.0	1.39	42.9	0.061
283	39	0	15.0	0.0	0.0	KIM	6.8	0.38	42.3	0.017
284	39	0	16.0	0.0	0.0	KIM	6.1	3.50	43.4	0.152
285	39	0	17.0	0.0	0.0	KIM	5.8	4.45	43.9	0.192
286	39	0	18.0	0.0	0.0	KIM	5.4	2.43	44.1	0.104
287	39	0	19.0	0.0	0.0	KIM	5.0	2.60	45.4	0.108
288	39	0	20.0	0.0	0.0	KIM	4.3	1.22	44.7	0.052
297	40	0	5.0	0.0	0.0	KIM	4.7	0.17	43.5	0.007
298	40	0	6.0	0.0	0.0	KIM	6.7	0.44	37.6	0.022
308	40	0	16.0	0.0	0.0	KIM	6.2	0.51	42.6	0.023
309	40	0	17.0	0.0	0.0	KIM	6.1	0.25	43.3	0.011
310	40	0	18.0	0.0	0.0	KIM	6.0	0.00	44.2	0.000
323	41	0	4.0	0.0	0.0	KIM	3.6	0.33	17.5	0.036
324	41	0	5.0	0.0	0.0	KIM	4.2	0.19	33.0	0.011
335	41	0	16.0	0.0	0.0	KIM	4.0	0.71	34.2	0.039
336	41	0	17.0	0.0	0.0	KIM	3.3	0.62	33.7	0.035
374	43	0	9.0	0.0	0.0	KIM	9.0	0.16	28.1	0.011
419	47	0	4.0	0.0	0.0	KIM	5.0	0.62	16.9	0.069
420	47	0	5.0	0.0	0.0	KIM	5.5	0.95	16.8	0.107
421	47	0	6.0	0.0	0.0	KIM	6.2	1.27	16.5	0.146
422	47	0	7.0	0.0	0.0	KIM	6.6	2.90	16.2	0.339
161	33	0	5.0	0.0	0.0	KIG	6.9	0.71	23.0	0.058
162	33	0	6.0	0.0	0.0	KIG	7.8	1.02	23.1	0.084
163	33	0	7.0	0.0	0.0	KIG	8.7	0.56	22.4	0.047
164	33	0	8.0	0.0	0.0	KIG	9.0	0.39	21.7	0.034
165	33	0	9.0	0.0	0.0	KIG	9.3	0.51	22.2	0.043
166	33	0	10.0	0.0	0.0	KIG	9.9	0.67	22.2	0.057

167	33	0	11.0	0.0	0.0	KIG	9.4	0.24	24.4	0.019
187	34	0	7.0	0.0	0.0	KIG	6.3	0.26	31.7	0.015
209	36	0	6.0	0.0	0.0	KIG	6.2	0.46	32.1	0.027
322	41	0	3.0	0.0	0.0	KIG	2.9	0.63	17.9	0.067
346	42	0	4.0	0.0	0.0	KIG	5.2	0.86	30.5	0.053
347	42	0	5.0	0.0	0.0	KIG	6.1	0.68	27.6	0.046
348	42	0	6.0	0.0	0.0	KIG	6.7	0.64	26.4	0.046
349	42	0	7.0	0.0	0.0	KIG	7.1	0.44	25.9	0.032
350	42	0	8.0	0.0	0.0	KIG	7.3	0.26	24.7	0.020
351	42	0	9.0	0.0	0.0	KIG	7.3	0.62	29.6	0.040
352	42	0	10.0	0.0	0.0	KIG	7.4	0.84	30.2	0.053
392	44	0	3.0	0.0	0.0	KIG	3.9	1.01	33.4	0.057
393	44	0	4.0	0.0	0.0	KIG	5.4	1.08	32.7	0.062
394	44	0	5.0	0.0	0.0	KIG	6.6	1.27	31.5	0.076
395	44	0	6.0	0.0	0.0	KIG	7.4	1.27	31.3	0.077
396	44	0	7.0	0.0	0.0	KIG	8.1	1.04	26.9	0.073
397	44	0	8.0	0.0	0.0	KIG	8.1	0.96	29.3	0.062
398	44	0	9.0	0.0	0.0	KIG	8.6	0.73	29.2	0.047
432	47	0	17.0	0.0	0.0	KIG	5.6	0.71	16.9	0.079
433	47	0	18.0	0.0	0.0	KIG	5.0	0.72	16.9	0.080
434	47	0	19.0	0.0	0.0	KIG	4.3	0.43	17.1	0.048
465	51	0	5.0	0.0	0.0	KIG	5.1	0.79	33.2	0.045
466	51	0	6.0	0.0	0.0	KIG	5.0	0.71	33.2	0.040
467	51	0	7.0	0.0	0.0	KIG	5.0	0.40	32.9	0.023
468	51	0	8.0	0.0	0.0	KIG	5.2	0.30	32.3	0.018
476	51	0	16.0	0.0	0.0	KIG	5.7	0.78	31.9	0.046
477	51	0	17.0	0.0	0.0	KIG	5.4	0.74	33.0	0.042
478	51	0	18.0	0.0	0.0	KIG	5.2	1.01	31.0	0.061
160	33	0	4.0	0.0	0.0	KIS	6.3	0.88	23.3	0.071
188	34	0	8.0	0.0	0.0	KIS	6.7	0.31	31.1	0.019
195	34	0	15.0	0.0	0.0	KIS	7.0	0.78	30.2	0.049
196	34	0	16.0	0.0	0.0	KIS	6.5	0.59	31.2	0.036
197	34	0	17.0	0.0	0.0	KIS	6.2	0.58	31.4	0.035
232	37	0	6.0	0.0	0.0	KIS	6.2	0.98	22.7	0.082
233	37	0	7.0	0.0	0.0	KIS	6.5	0.90	22.1	0.077
234	37	0	8.0	0.0	0.0	KIS	6.7	0.78	21.2	0.070
271	39	0	3.0	0.0	0.0	KIS	4.0	2.14	43.2	0.094
276	39	0	8.0	0.0	0.0	KIS	7.8	1.43	34.0	0.079
281	39	0	13.0	0.0	0.0	KIS	8.0	0.58	40.6	0.027
301	40	0	9.0	0.0	0.0	KIS	7.4	0.51	40.9	0.024
326	41	0	7.0	0.0	0.0	KIS	5.1	0.74	2.3	0.597
368	43	0	3.0	0.0	0.0	KIS	3.3	0.49	10.8	0.086
380	43	0	15.0	0.0	0.0	KIS	7.5	0.89	29.5	0.057
381	43	0	16.0	0.0	0.0	KIS	6.9	0.53	29.9	0.034
382	43	0	17.0	0.0	0.0	KIS	6.6	0.00	23.5	0.000
383	43	0	18.0	0.0	0.0	KIS	5.3	0.00	25.3	0.000
384	43	0	19.0	0.0	0.0	KIS	3.9	0.36	28.9	0.024
385	43	0	20.0	0.0	0.0	KIS	3.6	1.24	33.7	0.069
386	43	0	21.0	0.0	0.0	KIS	3.2	1.06	33.6	0.060
405	44	0	16.0	0.0	0.0	KIS	7.5	0.41	29.7	0.026
430	47	0	15.0	0.0	0.0	KIS	6.2	0.44	15.8	0.053

440	50	0	5.0	0.0	0.0	KIS	6.5	0.37	27.6	0.025
452	50	0	17.0	0.0	0.0	KIS	5.8	0.70	30.7	0.043
454	50	0	19.0	0.0	0.0	KIS	5.0	0.51	31.9	0.030
455	50	0	20.0	0.0	0.0	KIS	4.9	0.39	28.8	0.026
456	50	0	21.0	0.0	0.0	KIS	4.2	0.69	31.0	0.042
457	50	0	22.0	0.0	0.0	KIS	3.0	0.77	34.1	0.043
474	51	0	14.0	0.0	0.0	KIS	5.4	0.42	31.7	0.025
181	34	0	1.0	0.0	0.0	MJK	2.3	0.91	34.1	0.050
356	42	0	14.0	0.0	0.0	MJK	7.5	0.41	14.7	0.053
357	42	0	15.0	0.0	0.0	MJK	6.8	0.86	30.4	0.053
358	42	0	16.0	0.0	0.0	MJK	5.8	0.79	31.1	0.048
359	42	0	17.0	0.0	0.0	MJK	4.7	0.58	32.3	0.034
360	42	0	18.0	0.0	0.0	MJK	4.4	1.00	31.8	0.059
361	42	0	19.0	0.0	0.0	MJK	4.1	1.13	32.2	0.066
362	42	0	20.0	0.0	0.0	MJK	2.9	0.64	11.2	0.108
409	44	0	20.0	0.0	0.0	KJS	5.0	0.75	28.5	0.050
410	44	0	21.0	0.0	0.0	KJS	4.3	1.18	33.4	0.067
411	44	0	22.0	0.0	0.0	KJS	3.3	1.82	17.7	0.195
47	24	0	12.0	0.0	0.0	LIS	1.0	1.48	49.8	0.056
48	24	0	13.0	0.0	0.0	LIS	1.2	0.61	49.7	0.023
49	24	0	14.0	0.0	0.0	LIS	1.3	0.36	49.6	0.014
90	28	0	6.0	0.0	0.0	LIS	0.7	1.12	36.7	0.058
91	28	0	7.0	0.0	0.0	LIS	0.7	0.87	36.8	0.045
17	19	0	11.0	0.0	0.0	LCS	0.4	0.88	49.2	0.034
32	22	0	11.0	0.0	0.0	LCS	1.5	0.60	49.6	0.023
33	22	0	13.0	0.0	0.0	LCS	1.3	0.43	49.5	0.016
171	33	0	15.0	0.0	0.0	LCS	9.3	0.12	27.0	0.008
27	21	0	4.0	0.0	0.0	LIG	2.2	0.51	48.8	0.020
4	17	0	6.0	0.0	0.0	MMA	0.7	0.94	49.9	0.036
6	18	1	5.0	0.0	0.0	MMA	0.4	1.16	49.6	0.044
9	18	0	11.0	0.0	0.0	MMA	0.6	0.83	49.1	0.032
18	19	0	13.0	0.0	0.0	MMA	0.4	0.47	49.2	0.018
23	20	0	9.0	0.0	0.0	MMA	0.4	0.65	50.4	0.024
26	21	1	2.0	0.0	0.0	MMA	0.8	0.86	49.8	0.033
34	22	0	15.0	0.0	0.0	MMA	0.8	0.40	49.7	0.015
50	24	0	16.0	0.0	0.0	MMA	0.8	0.55	49.8	0.021
87	28	0	3.0	0.0	0.0	MMA	0.3	0.28	37.1	0.014
100	28	0	16.0	0.0	0.0	MMA	1.1	0.22	36.2	0.011
101	28	0	17.0	0.0	0.0	MMA	0.9	0.24	36.4	0.012
102	28	0	18.0	0.0	0.0	MMA	0.3	0.19	37.1	0.010
105	29	1	6.0	0.0	0.0	MMA	1.6	1.99	48.5	0.078
106	29	0	7.0	0.0	0.0	MMA	1.8	1.52	48.2	0.060
107	29	0	8.0	0.0	0.0	MMA	1.7	1.24	48.4	0.048
108	29	0	9.0	0.0	0.0	MMA	1.9	1.17	48.1	0.046
109	29	0	10.0	0.0	0.0	MMA	1.7	1.30	48.4	0.051

110	29	0	11.0	0.0	0.0	MMA	1.5	1.08	48.7	0.042
111	29	0	12.0	0.0	0.0	MMA	1.2	1.24	49.1	0.048
112	29	0	13.0	0.0	0.0	MMA	0.9	0.60	49.6	0.023
113	29	0	14.0	0.0	0.0	MMA	0.5	0.35	50.2	0.013
129	30	0	12.0	0.0	0.0	MMA	0.8	1.72	49.3	0.066
130	30	0	13.0	0.0	0.0	MMA	0.9	0.79	49.2	0.030
136	31	0	2.0	0.0	0.0	MMA	0.3	0.38	50.5	0.014
137	31	0	3.0	0.0	0.0	MMA	0.3	0.44	50.5	0.016
138	31	0	4.0	0.0	0.0	MMA	0.4	0.54	50.4	0.020
139	31	0	5.0	0.0	0.0	MMA	0.3	0.46	50.5	0.017
140	31	0	6.0	0.0	0.0	MMA	0.3	0.60	50.5	0.022
141	31	0	8.0	0.0	0.0	MMA	0.3	0.54	50.5	0.020
142	31	0	9.0	0.0	0.0	MMA	0.3	0.24	50.5	0.009
143	31	0	10.0	0.0	0.0	MMA	0.4	0.19	50.4	0.007
144	31	0	11.0	0.0	0.0	MMA	0.4	0.32	50.4	0.012
145	31	0	12.0	0.0	0.0	MMA	0.3	0.33	50.5	0.012
146	31	0	13.0	0.0	0.0	MMA	0.3	0.26	50.5	0.010
147	31	0	14.0	0.0	0.0	MMA	0.3	0.41	50.5	0.015
152	32	0	2.0	0.0	0.0	MMA	0.3	0.16	19.2	0.016
153	32	0	3.0	0.0	0.0	MMA	0.4	0.23	19.2	0.023
154	32	0	4.0	0.0	0.0	MMA	0.4	0.18	19.2	0.018
155	32	0	5.0	0.0	0.0	MMA	0.5	0.35	19.1	0.035
158	33	0	2.0	0.0	0.0	MMA	4.0	1.00	26.0	0.073
177	33	0	21.0	0.0	0.0	MMA	4.5	0.38	25.7	0.028
178	33	0	22.0	0.0	0.0	MMA	1.3	0.73	28.3	0.049
223	36	0	20.0	0.0	0.0	MMA	1.7	0.56	35.3	0.030
224	36	0	21.0	0.0	0.0	MMA	1.2	1.36	35.9	0.072
228	37	0	2.0	0.0	0.0	MMA	3.5	0.80	24.9	0.061
247	37	0	21.0	0.0	0.0	MMA	0.9	0.61	27.0	0.043
266	38	0	19.0	0.0	0.0	MMA	1.2	2.87	49.2	0.110
270	39	0	2.0	0.0	0.0	MMA	3.0	1.49	45.9	0.061
291	39	0	24.0	0.0	0.0	MMA	1.8	2.22	48.3	0.087
294	40	0	2.0	0.0	0.0	MMA	3.2	0.65	19.1	0.064
314	40	0	22.0	0.0	0.0	MMA	2.3	0.52	47.5	0.021
387	43	0	22.0	0.0	0.0	MMA	1.6	1.49	34.8	0.081
437	50	0	2.0	0.0	0.0	MMA	3.0	1.81	33.7	0.101
458	50	0	23.0	0.0	0.0	MMA	1.9	0.80	34.8	0.043
484	52	0	1.0	0.0	0.0	MMA	0.8	0.46	26.4	0.033
485	52	0	2.0	0.0	0.0	MMA	0.9	0.40	26.3	0.029
486	52	0	3.0	0.0	0.0	MMA	0.9	0.46	26.3	0.033
487	52	0	4.0	0.0	0.0	MMA	0.9	0.45	26.3	0.032
488	52	0	5.0	0.0	0.0	MMA	1.0	0.53	26.2	0.038
489	52	0	6.0	0.0	0.0	MMA	1.0	0.74	26.4	0.053
490	52	0	7.0	0.0	0.0	MMA	1.1	0.66	26.2	0.048
491	52	0	8.0	0.0	0.0	MMA	1.3	0.55	26.0	0.040
492	52	0	9.0	0.0	0.0	MMA	1.1	0.52	26.2	0.037
493	52	0	10.0	0.0	0.0	MMA	1.0	0.62	26.1	0.045
494	52	0	11.0	0.0	0.0	MMA	1.0	0.95	26.1	0.069
498	52	0	15.0	0.0	0.0	MMA	0.8	0.51	26.4	0.037
499	52	0	16.0	0.0	0.0	MMA	0.5	0.48	26.6	0.034
500	52	0	17.0	0.0	0.0	MMA	0.5	0.36	26.6	0.026

14	19	0	5.0	0.0	0.0	MJS	1.0	0.76	49.5	0.029
194	34	0	14.0	0.0	0.0	MJS	7.9	0.62	29.5	0.040
367	43	0	2.0	0.0	0.0	MJS	3.0	0.64	11.1	0.109
19	20	1	1.0	0.0	0.0	DJM	0.2	0.39	50.9	0.014
20	20	0	3.0	0.0	0.0	DJM	0.2	0.49	50.9	0.018
21	20	0	5.0	0.0	0.0	DJM	0.3	0.59	50.7	0.022
22	20	0	7.0	0.0	0.0	DJM	0.5	0.58	49.8	0.022
24	20	0	11.0	0.0	0.0	DJM	0.2	0.45	50.9	0.017
55	25	0	2.0	0.0	0.0	DJM	0.3	0.96	50.5	0.036
56	25	0	3.0	0.0	0.0	DJM	0.2	0.86	50.9	0.032
57	25	0	4.0	0.0	0.0	DJM	0.3	0.50	50.7	0.019
58	25	0	5.0	0.0	0.0	DJM	0.3	0.47	50.7	0.018
59	25	0	6.0	0.0	0.0	DJM	0.3	0.72	50.7	0.027
60	25	0	7.0	0.0	0.0	DJM	0.2	0.59	50.9	0.022
61	25	0	8.0	0.0	0.0	DJM	0.3	0.62	50.7	0.023
62	25	0	9.0	0.0	0.0	DJM	0.3	0.63	50.7	0.023
63	25	0	10.0	0.0	0.0	DJM	0.4	0.34	50.3	0.013
64	25	0	11.0	0.0	0.0	DJM	0.3	0.46	50.7	0.017
65	25	0	12.0	0.0	0.0	DJM	0.2	0.33	50.9	0.012
66	25	0	13.0	0.0	0.0	DJM	0.4	0.42	50.4	0.016
67	25	0	14.0	0.0	0.0	DJM	0.5	0.38	50.2	0.014
68	25	0	15.0	0.0	0.0	DJM	0.6	0.68	48.5	0.027
99	28	0	15.0	0.0	0.0	DJM	0.6	0.30	36.7	0.015
114	29	0	15.0	0.0	0.0	DJM	0.6	0.32	50.0	0.012
118	30	0	1.0	0.0	0.0	DJM	0.8	0.76	49.5	0.029
119	30	0	2.0	0.0	0.0	DJM	0.7	0.53	49.7	0.020
120	30	0	3.0	0.0	0.0	DJM	0.6	0.48	49.9	0.018
121	30	0	4.0	0.0	0.0	DJM	0.6	1.30	49.9	0.049
122	30	0	5.0	0.0	0.0	DJM	0.5	1.46	50.2	0.055
123	30	0	6.0	0.0	0.0	DJM	0.5	1.28	50.2	0.048
124	30	0	7.0	0.0	0.0	DJM	0.6	1.27	49.9	0.048
125	30	0	8.0	0.0	0.0	DJM	0.7	1.16	49.7	0.044
126	30	0	9.0	0.0	0.0	DJM	0.6	1.37	49.9	0.052
127	30	0	10.0	0.0	0.0	DJM	0.6	2.02	49.9	0.076
128	30	0	11.0	0.0	0.0	DJM	0.7	2.44	49.7	0.093
131	30	0	14.0	0.0	0.0	DJM	0.7	0.50	49.7	0.019
132	30	0	15.0	0.0	0.0	DJM	0.6	0.47	50.0	0.018
133	30	0	16.0	0.0	0.0	DJM	0.4	0.85	50.4	0.032
135	31	1	1.0	0.0	0.0	DJM	0.2	0.43	50.9	0.016
148	31	0	15.0	0.0	0.0	DJM	0.6	0.45	50.0	0.017
227	37	1	1.0	0.0	0.0	DJM	1.2	0.91	26.3	0.065
35	23	1	1.0	0.0	0.0	MJF	1.3	0.56	49.0	0.022
72	26	0	1.0	0.0	0.0	MJF	1.0	0.76	50.0	0.029
304	40	0	12.0	0.0	0.0	MJF	6.8	0.39	2.6	0.284
43	23	0	16.0	0.0	0.0	WJM	1.0	0.12	49.4	0.005
103	28	0	19.0	0.0	0.0	MJD	0.2	0.46	37.3	0.023
149	31	0	16.0	0.0	0.0	MJD	0.1	0.37	51.2	0.014
317	40	0	25.0	0.0	0.0	MJD	0.3	0.95	50.7	0.035
159	33	0	3.0	0.0	0.0	MJC	5.0	0.87	25.0	0.066
190	34	0	10.0	0.0	0.0	MMB	8.3	0.52	29.2	0.034
192 *	34	0	12.0	0.0	0.0	MMB	8.5	0.47	6.7	0.133

255	38	0	6.0	0.0	0.0	MMB	4.5	0.58	44.6	0.025
256	38	0	7.0	0.0	0.0	MMB	4.3	0.30	44.8	0.013
257	38	0	9.0	0.0	0.0	MMB	4.0	0.10	45.2	0.004
258*	38	0	10.0	0.0	0.0	MMB	3.9	0.47	9.5	0.093
259*	38	0	11.0	0.0	0.0	MMB	4.0	0.78	9.3	0.159
260	38	0	12.0	0.0	0.0	MMB	4.2	1.20	45.0	0.050
261	38	0	13.0	0.0	0.0	MMB	4.5	1.35	45.0	0.057
262	38	0	14.0	0.0	0.0	MMB	4.2	1.07	45.0	0.045
302	40	0	10.0	0.0	0.0	MMB	7.6	0.42	40.6	0.020
327	41	0	8.0	0.0	0.0	MMB	5.3	0.60	2.3	0.485
328*	41	0	9.0	0.0	0.0	MMB	5.2	0.28	0.7	0.779
329*	41	0	10.0	0.0	0.0	MMB	5.1	0.39	0.5	1.532
330*	41	0	11.0	0.0	0.0	MMB	5.1	0.19	0.6	0.592
331	41	0	12.0	0.0	0.0	MMB	5.0	0.41	2.4	0.328
332	41	0	13.0	0.0	0.0	MMB	5.0	0.27	2.4	0.216
428*	47	0	13.0	0.0	0.0	MMB	6.5	0.51	4.4	0.221
429	47	0	14.0	0.0	0.0	MMB	6.5	0.44	15.9	0.052
447*	50	0	12.0	0.0	0.0	MMB	8.1	0.65	8.2	0.149
448*	50	0	13.0	0.0	0.0	MMB	7.8	0.59	2.4	0.459
449*	50	0	14.0	0.0	0.0	MMB	7.0	0.62	5.3	0.221
470	51	0	10.0	0.0	0.0	MMB	5.3	0.41	32.9	0.024
471*	51	0	11.0	0.0	0.0	MMB	5.6	0.54	2.3	0.438
473	51	0	13.0	0.0	0.0	MMB	5.1	0.38	32.0	0.022
191	34	0	11.0	0.0	0.0	MJB	8.2	1.20	7.5	0.301
193	34	0	13.0	0.0	0.0	MJB	8.1	0.52	29.3	0.034
14	19	0	5.0	0.0	0.0	MJS	1.0	0.76	49.5	0.029
194	34	0	14.0	0.0	0.0	MJS	7.9	0.62	29.5	0.040
367	43	0	2.0	0.0	0.0	MJS	3.0	0.64	11.1	0.109
201	34	0	21.0	0.0	0.0	PJM	1.4	1.02	35.0	0.055
246	37	0	20.0	0.0	0.0	PJM	1.9	0.47	26.2	0.034
254	38	0	5.0	0.0	0.0	AJM	3.0	0.39	17.7	0.042
181	34	0	1.0	0.0	0.0	MJK	2.3	0.91	34.1	0.050
356	42	0	14.0	0.0	0.0	MJK	7.5	0.41	14.7	0.053
357	42	0	15.0	0.0	0.0	MJK	6.8	0.86	30.4	0.053
358	42	0	16.0	0.0	0.0	MJK	5.8	0.79	31.1	0.048
359	42	0	17.0	0.0	0.0	MJK	4.7	0.58	32.3	0.034
360	42	0	18.0	0.0	0.0	MJK	4.4	1.00	31.8	0.059
361	42	0	19.0	0.0	0.0	MJK	4.1	1.13	32.2	0.066
362	42	0	20.0	0.0	0.0	MJK	2.9	0.64	11.2	0.108
355	42	0	13.0	0.0	0.0	CJM	7.8	2.45	5.5	0.839
363	42	0	21.0	0.0	0.0	MJA	2.2	0.56	11.5	0.092
198	34	0	18.0	0.0	0.0	PLG	5.6	0.46	33.0	0.026
199	34	0	19.0	0.0	0.0	PLG	5.4	0.39	33.3	0.022
200	34	0	20.0	0.0	0.0	PLG	3.5	0.81	33.7	0.045
221	36	0	18.0	0.0	0.0	PLG	5.0	1.60	30.7	0.098
222	36	0	19.0	0.0	0.0	PLG	3.8	1.06	33.1	0.060
245	37	0	19.0	0.0	0.0	PLG	3.8	0.52	25.4	0.039
265	38	0	18.0	0.0	0.0	PLG	1.9	0.91	48.8	0.035

339	41	0	20.0	0.0	0.0	PLG	1.2	1.47	36.4	0.076
343	42	0	1.0	0.0	0.0	PLG	2.0	0.72	34.5	0.039
480	51	0	20.0	0.0	0.0	PLG	4.3	1.46	32.9	0.084
481	51	0	21.0	0.0	0.0	PLG	2.8	0.55	17.8	0.058
201	34	0	21.0	0.0	0.0	PJM	1.4	1.02	35.0	0.055
246	37	0	20.0	0.0	0.0	PJM	1.9	0.47	26.2	0.034

15	19	0	7.0	0.0	0.0	SIG	0.7	0.70	50.2	0.026
28	21	0	6.0	0.0	0.0	SIG	3.0	0.59	48.3	0.023
42	23	0	14.0	0.0	0.0	SIG	3.9	0.62	48.1	0.024
77	26	0	6.0	0.0	0.0	SIG	3.2	1.32	48.3	0.052
78	26	0	7.0	0.0	0.0	SIG	3.8	1.96	47.8	0.077
95	28	0	11.0	0.0	0.0	SIG	1.0	0.60	19.0	0.060
96	28	0	12.0	0.0	0.0	SIG	1.0	0.36	19.0	0.036
97	28	0	13.0	0.0	0.0	SIG	1.1	0.13	19.0	0.013
251	38	0	2.0	0.0	0.0	SIG	0.8	0.42	18.9	0.042
438	50	0	3.0	0.0	0.0	SIG	3.3	1.06	17.8	0.113
36	23	0	3.0	0.0	0.0	SIS	3.2	0.81	48.3	0.032
40	23	0	10.0	0.0	0.0	SIS	4.2	0.96	43.4	0.042
75	26	0	4.0	0.0	0.0	SIS	2.4	0.10	48.8	0.004
76	26	0	5.0	0.0	0.0	SIS	2.8	0.41	48.7	0.016
79	26	0	8.0	0.0	0.0	SIS	3.9	0.66	47.7	0.026
80	26	0	9.0	0.0	0.0	SIS	3.8	0.91	47.9	0.036
312	40	0	20.0	0.0	0.0	SIS	5.4	0.00	39.2	0.000
313	40	0	21.0	0.0	0.0	SIS	5.0	0.36	40.5	0.017
412	44	0	23.0	0.0	0.0	SIS	2.8	1.85	6.7	0.519
413	44	0	24.0	0.0	0.0	SIS	1.8	0.53	6.8	0.147
424	47	0	9.0	0.0	0.0	SIS	6.0	3.08	6.0	0.963
425	47	0	10.0	0.0	0.0	SIS	6.0	1.04	6.1	0.324
439	50	0	4.0	0.0	0.0	SIS	4.9	0.84	33.3	0.048
73	26	0	2.0	0.0	0.0	SIL	1.0	0.14	49.9	0.005
74	26	0	3.0	0.0	0.0	SIL	1.8	0.15	49.1	0.006
81	26	0	10.0	0.0	0.0	SIL	3.7	0.68	48.0	0.027
82	26	0	11.0	0.0	0.0	SIL	3.7	1.17	47.9	0.046
83	26	0	12.0	0.0	0.0	SIL	3.6	1.28	48.0	0.050
14	19	0	5.0	0.0	0.0	MJS	1.0	0.76	49.5	0.029
194	34	0	14.0	0.0	0.0	MJS	7.9	0.62	29.5	0.040
367	43	0	2.0	0.0	0.0	MJS	3.0	0.64	11.1	0.109
409	44	0	20.0	0.0	0.0	KJS	5.0	0.75	28.5	0.050
410	44	0	21.0	0.0	0.0	KJS	4.3	1.18	33.4	0.067
411	44	0	22.0	0.0	0.0	KJS	3.3	1.82	17.7	0.195

230	37	0	4.0	0.0	0.0	VES	5.7	1.17	24.1	0.092
231	37	0	5.0	0.0	0.0	VEG	6.0	1.17	19.5	0.113

264	38	0	16.0	0.0	0.0	WAT	3.7	0.77	47.8	0.030
289	39	0	22.0	0.0	0.0	WAT	3.2	2.32	48.3	0.091
1	17	1	0.0	0.0	0.0	WJD	0.0	0.08	52.1	0.003
53	25	1	0.0	0.0	0.0	WJD	0.0	0.58	52.1	0.021
71	26	1	0.0	0.0	0.0	WJD	0.0	0.72	52.1	0.026
84	28	1	0.0	0.0	0.0	WJD	0.0	0.75	38.2	0.037
117	30	1	0.0	0.0	0.0	WJD	0.0	0.85	52.1	0.031
150	32	1	0.0	0.0	0.0	WJD	0.0	0.08	19.8	0.008
156	33	1	0.0	0.0	0.0	WJD	0.0	0.71	30.2	0.044
180	34	1	0.0	0.0	0.0	WJD	0.0	1.29	38.2	0.064
203	36	1	0.0	0.0	0.0	WJD	0.0	0.73	38.2	0.036
249	38	1	0.0	0.0	0.0	WJD	0.0	1.11	19.8	0.106
268	39	1	0.0	0.0	0.0	WJD	0.0	0.39	52.1	0.014
292	40	1	0.0	0.0	0.0	WJD	0.0	0.47	21.4	0.042
319	41	1	0.0	0.0	0.0	WJD	0.0	1.14	19.8	0.109
342	42	1	0.0	0.0	0.0	WJD	0.0	0.84	38.2	0.042
365	43	1	0.0	0.0	0.0	WJD	0.0	0.73	12.9	0.107
435	50	1	0.0	0.0	0.0	WJD	0.0	0.20	38.2	0.010
11	18	0	15.0	0.0	0.0	DJW	0.0	0.38	52.1	0.014
52	24	0	18.0	0.0	0.0	DJW	0.0	0.72	52.1	0.026
70	25	0	17.0	0.0	0.0	DJW	0.0	0.88	52.1	0.032
104	28	0	20.0	0.0	0.0	DJW	0.0	0.22	38.2	0.011
116	29	0	17.0	0.0	0.0	DJW	0.0	0.18	52.1	0.007
134	30	0	17.0	0.0	0.0	DJW	0.0	1.12	52.1	0.041
179	33	0	23.0	0.0	0.0	DJW	0.0	0.39	30.2	0.024
202	34	0	22.0	0.0	0.0	DJW	0.0	0.69	38.2	0.034
226	36	0	23.0	0.0	0.0	DJW	0.0	0.46	38.2	0.023
248	37	0	22.0	0.0	0.0	DJW	0.0	0.25	28.3	0.017
318	40	0	26.0	0.0	0.0	DJW	0.0	0.70	52.1	0.025
341	41	0	22.0	0.0	0.0	DJW	0.0	1.11	19.8	0.106
459	50	0	24.0	0.0	0.0	DJW	0.0	0.45	38.2	0.022
460	51	1	0.0	0.0	0.0	DJW	0.0	0.69	19.8	0.066
483	52	1	0.0	0.0	0.0	DJW	0.0	0.14	28.3	0.009
502	53	1	0.0	0.0	0.0	DJW	0.0	0.35	19.8	0.033
43	23	0	16.0	0.0	0.0	WJM	1.0	0.12	49.4	0.005